

## 1

# Solar-like Oscillations: An Observational Perspective

**Timothy R. Bedding**

Sydney Institute for Astronomy (SIfA), School of Physics, University of Sydney, Australia

## 1.1 What are solar-like oscillations?

Oscillations in the Sun are excited stochastically by convection. We use the term *solar-like* to refer to oscillations in other stars that are excited by the same mechanism, even though some of these stars may be very different from the Sun. The stochastic nature of the excitation produces oscillations over a broad range of frequencies, which in the Sun is about 1 to 4 mHz (the well-known 5-minute oscillations). Stellar oscillations can also be excited via opacity variations (the *heat-engine mechanism*, also called the  $\kappa$  mechanism), as seen in various types of classical pulsating stars (Cepheids, RR Lyraes, Miras, white dwarfs,  $\delta$  Scuti stars, etc.).

For a star to show solar-like oscillations it must be cool enough to have a surface convective zone. In practice, this means being cooler than the red edge of the classical instability strip, which includes the lower main sequence, as well as cool subgiants and even red giants. Indeed, solar-like oscillations with periods of hours (and longer) have now been observed in thousands of G and K giants (see Sec. 1.9). There is also good evidence that the pulsations in semiregular variables (M giants) are solar-like (Christensen-Dalsgaard et al., 2001; Bedding, 2003; Tabur et al., 2010), as perhaps are those in M supergiants such as Betelgeuse (Kiss et al., 2006).

What about hotter stars? By definition, solar-like oscillations are excited stochastically in the outer convection zone. Given that surface convection is thought to inhibit operation of the  $\kappa$  mechanism (e.g., Gastine and Dintrans, 2011), it seems that solar-like and heat-engine oscillations would be mutually exclusive. In fact, both may operate in a star provided the surface convection layer is thin (Samadi et al., 2002; Kallinger and Matthews, 2010) and there is evidence from *Kepler*

data for solar-like oscillations in at least one  $\delta$  Scuti star (Antoci et al., 2011). There has even been a suggestion that sub-surface convection in B-type stars could excite solar-like oscillations (Cantiello et al., 2009; Belkacem et al., 2010). There is some evidence from *CoRoT* observations that the  $\beta$  Cephei star V1449 Aql shows solar-like oscillations (Belkacem et al., 2009), although other interpretations are possible (Degroote et al., 2009) and *Kepler* observations of similar stars have so far failed to confirm stochastically-excited oscillations (Balona et al., 2011). Meanwhile, Degroote et al. (2010) suggested that the O-type star HD 46149 shows stochastically-excited oscillations, based on *CoRoT* photometry.

## 1.2 Properties of oscillations

We now summarise the main properties of solar-like oscillations. For more extensive discussion see, for example, Brown and Gilliland (1994), Bedding and Kjeldsen (2003), Christensen-Dalsgaard (2004), Ballot (2010) and Aerts et al. (2010).

### 1.2.1 Types of oscillation modes

Broadly speaking, there are two types of stellar oscillations. Pressure modes (*p modes*) are acoustic waves, for which the restoring force arises from the pressure gradient. These are seen in the Sun and sun-like stars, and also in most of the classical pulsators. For gravity modes (*g modes*) the restoring force is buoyancy. The best studied examples occur in white dwarfs (see Althaus et al., 2010, for a recent review), but g modes are also seen in other classical pulsators such as  $\gamma$  Dor stars, slowly pulsating B stars and some sdB stars. Some stars have been found to have both p modes and g modes, including hybrid  $\delta$  Scuti/ $\gamma$  Dor stars (Grigahcène et al., 2010) and possibly the Sun (García et al., 2008). Finally, some stars oscillate in *mixed modes*, which have p-mode character in the envelope and g-mode character in the core. These are discussed in Secs. 1.8 and 1.9. First, however, we consider p modes in some detail because they are most relevant to the topic of solar-like oscillations.

Mathematically, each p mode can be described by three integers. The *radial order* ( $n$ ) specifies the number of nodal shells of the standing wave. In the Sun, the modes with the highest amplitude have  $n$  in the range 19–22. The *angular degree* ( $l = 0, 1, 2, \dots$ ) specifies the number of nodal lines at the surface. Modes with  $l = 0$  are called *radial* modes

and those with  $l \geq 1$  are *non-radial* modes. In addition, modes with  $l = 0$  are sometimes called *monopole* modes, while those with  $l = 1$  are *dipole* modes, those with  $l = 2$  are *quadrupole* modes, and those with  $l = 3$  are *octupole* modes. Since the surface of a distant star is generally not resolved, cancellation effects mean that only modes with  $l \leq 3$  (or perhaps 4) are observable.

The third integer that specifies a mode is the *azimuthal order* ( $m$ ), which takes on values from  $-l$  to  $+l$ . However, the oscillation frequencies do not depend on  $m$  unless the star is rotating (or spherical symmetry is broken in some other way, such as by the presence of a magnetic field). For a rotating star, the modes with a given  $n$  and  $l$  are split in frequency into a multiplet with  $2l + 1$  components (one for each value of  $m$ ). The frequency separation between these components is proportional to the rotational frequency of the star and their relative amplitudes depend on the inclination angle between the stellar rotation axis and the line of sight. The study of rotational splitting in solar-like oscillations, while showing great promise, is still in its infancy and will not be discussed further in this chapter.

The comments in the preceding two paragraphs also apply to g modes, but note that (i) radial g modes do not exist (and, therefore, neither do radial mixed modes), (ii)  $n$  is generally taken to be negative for g modes (see Sec. 3.5.2 of Aerts et al. 2010 for a full discussion), and (iii) rotational splitting of g modes depends on  $l$  (Sec 3.8.4 of Aerts et al., 2010).

### 1.2.2 The frequency spectrum of oscillations

Figure 1.1a shows the frequency spectrum of p modes in the Sun. The envelope of the peak heights defines the frequency of maximum power,  $\nu_{\max}$ , which has a value of about  $3100 \mu\text{Hz}$  in the Sun. The mode frequencies show a very regular pattern that is characteristic of an oscillating sphere. Figure 1.1b shows a close-up labelled with the  $(n, l)$  values of the modes, which were determined by comparing with theoretical models. Note the alternating pattern of large and small separations as  $l$  cycles repeatedly through the values 2, 0, 3, 1, 2, 0, ... The quantity  $\Delta\nu$  is the spacing between consecutive radial overtones (that is, modes with a given  $l$  whose  $n$  values differ by 1). It is called the *large frequency separation* and has a value of  $135 \mu\text{Hz}$  in the Sun. To a good approximation,  $\Delta\nu$  is proportional to the square root of the mean stellar density (see Sec. 1.6).

In Fig. 1.1b we see two so-called *small frequency separations*:  $\delta\nu_{02}$  is

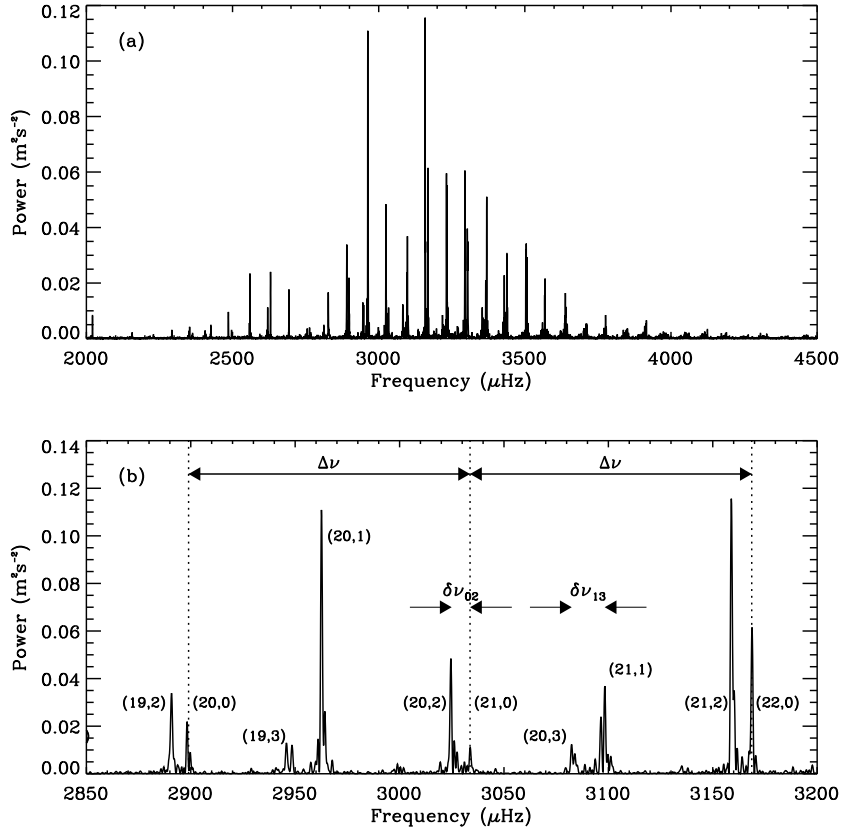


Figure 1.1 The solar power spectrum from ten days of disk-integrated velocity measurements with the BiSON instrument (e.g., Chaplin et al., 1997). Panel (b) shows a close-up labelled with  $(n, l)$  values for each mode. Dotted lines show the radial modes, and the large and small separations are indicated.

the spacing between close pairs with  $l = 0$  and  $l = 2$  (for which  $n$  differs by 1) and  $\delta\nu_{13}$  is the spacing between adjacent modes with  $l = 1$  and  $l = 3$  (ditto). Another small separation can be defined by noting that the  $l = 1$  modes do not fall exactly halfway between  $l = 0$  modes. We define  $\delta\nu_{01}$  to be the amount by which  $l = 1$  modes are offset from the midpoint of the  $l = 0$  modes on either side.<sup>1</sup> To be explicit, for a given

<sup>1</sup> One can also define an equivalent quantity,  $\delta\nu_{10}$ , as the offset of  $l = 0$  modes from the midpoint between the surrounding  $l = 1$  modes, so that  $\delta\nu_{10} = \nu_{n,0} - \frac{1}{2}(\nu_{n-1,1} + \nu_{n,1})$ .

radial order,  $n$ , these separations are defined as follows:

$$\delta\nu_{02} = \nu_{n,0} - \nu_{n-1,2} \quad (1.1)$$

$$\delta\nu_{01} = \frac{1}{2}(\nu_{n,0} + \nu_{n+1,0}) - \nu_{n,1} \quad (1.2)$$

$$\delta\nu_{13} = \nu_{n,1} - \nu_{n-1,3}. \quad (1.3)$$

In practice, the oscillation spectrum is not precisely regular and so all of these spacings vary slightly with frequency.

The  $l = 4$  modes are weakly visible in Fig. 1.1b (at 3000 and 3136  $\mu\text{Hz}$ ). By analogy with  $l = 2$ , we can define the small separation for these modes as

$$\delta\nu_{04} = \nu_{n,0} - \nu_{n-2,4}. \quad (1.4)$$

Finally, we note that each peak in the power spectrum in Fig. 1.1b is slightly broadened, which reflects the finite lifetimes of the modes. If we define the lifetime  $\tau$  of a damped oscillation mode to be the time for the amplitude to decay by a factor of  $e$  then this mode will produce a Lorentzian shape in the power spectrum with a linewidth (FWHM) of  $\Gamma = (\pi\tau)^{-1}$ . The dominant modes in the Sun have linewidths of 1–2  $\mu\text{Hz}$  and hence lifetimes of 2–4 days (e.g., Chaplin et al., 1997).

### 1.2.3 The échelle diagram

The échelle diagram, first introduced by Grec et al. (1983) for global helioseismology, is used extensively in asteroseismology to display oscillation frequencies. It involves dividing the spectrum into equal segments of length  $\Delta\nu$  and stacking them one above the other so that modes with a given degree align vertically in ridges. Any departures from regularity are clearly visible as curvature in the échelle diagram. For example, variations in the small separations appear as a convergence or divergence of the corresponding ridges.

Figure 1.2 shows the observed frequencies in the Sun in échelle format for modes with  $l \leq 4$  (filled symbols), using a large separation of  $\Delta\nu = 135.0 \mu\text{Hz}$ . Using a slightly smaller value of  $\Delta\nu$  causes the ridges to tilt to the right, as shown by the open symbols for  $l = 0$  only. It also shifts the ridges sideways, which is important if we are trying to measure the quantity  $\epsilon$  (see Sec. 1.2.4).

Sometimes the ridges wrap around, which has almost happened to the  $l = 1$  modes at the top of Fig. 1.2 (filled triangles). Of course, the diagram can be made wider by plotting the ridges more than once (an example is shown in the right panel of Fig. 1.10). Also note that one

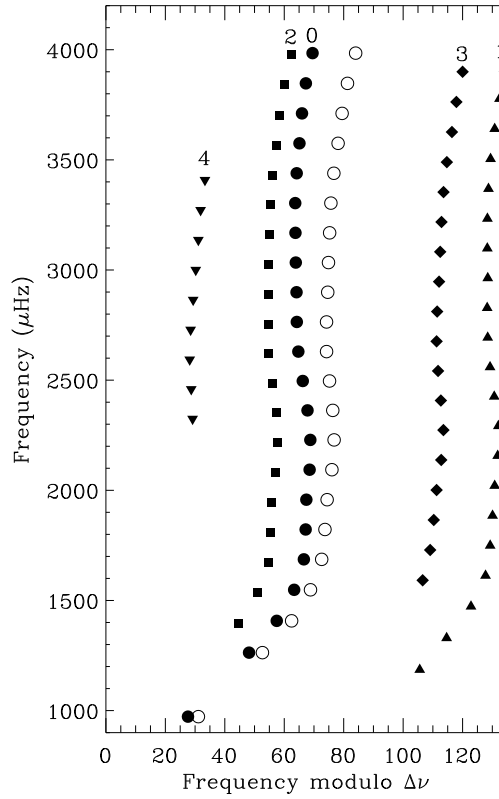


Figure 1.2 Échelle diagram of the observed frequencies in the Sun (Broomhall et al., 2009). The filled symbols show the frequencies of modes with  $l = 0, 1, 2, 3$  and  $4$ , using a large separation of  $\Delta\nu = 135.0 \mu\text{Hz}$ . The open symbols show the result of plotting the  $l = 0$  frequencies modulo a slightly smaller large separation ( $\Delta\nu = 134.5 \mu\text{Hz}$ ).

can shift the ridges sideways by subtracting a fixed reference frequency, which must be kept in mind when reading  $\epsilon$  from the diagram (again, see Fig. 1.10).

When making an échelle diagram, it is usual to plot  $\nu$  versus  $(\nu \bmod \Delta\nu)$ , in which case each order slopes upwards slightly (see Fig. 1.2). However, for greyscale images it can be preferable to keep the orders horizontal (an example is shown Fig. 1.4).

### 1.2.4 The asymptotic relation

The approximate regularity of the p-mode spectrum means we can express the mode frequencies in terms of the large and small separations, as follows:

$$\nu_{n,l} \approx \Delta\nu(n + \frac{1}{2}l + \epsilon) - \delta\nu_{0l}. \quad (1.5)$$

Here,  $\nu_{n,l}$  is the frequency of the p mode with radial order  $n$  and angular degree  $l$  (and assuming no dependence on  $m$ , which means neglecting any rotational splitting). By definition, the small separation  $\delta\nu_{0l}$  is zero for  $l = 0$ . Its values for  $l = 1, 2$  and  $4$  have already been discussed (Eqs. 1.1, 1.2, and 1.4). For  $l = 3$  we have  $\delta\nu_{03} = \delta\nu_{01} + \delta\nu_{13}$ , and we note that  $\delta\nu_{03}$  is the amount by which the  $l = 3$  mode is offset from the midpoint of the adjacent  $l = 0$  modes. This is arguably a more sensible measurement of the position of the  $l = 3$  ridge than  $\delta\nu_{13}$  because it is made with reference to the radial modes (see Bedding et al., 2010b).

Equation 1.5 describes the oscillation frequencies from an observational perspective. A theoretical asymptotic expression (Tassoul, 1980; Gough, 1986, 2003) gives physical significance to  $\Delta\nu$ ,  $\delta\nu_{0l}$  and  $\epsilon$  as integrals of the sound speed. It turns out that the large separation is approximately proportional to the square root of the mean stellar density, as discussed further in Sec. 1.6. The small separations in main-sequence stars are sensitive to the gradient of the sound speed near the core, and hence to the age of the star (see Sec. 1.7). The asymptotic analysis (see previous references) indicates that  $\delta\nu_{0l}$  is proportional to  $l(l+1)$ . Finally,  $\epsilon$  is sensitive to upper turning point of the modes (e.g., Gough, 1986; Pérez Hernández and Christensen-Dalsgaard, 1998; Roxburgh, 2010). In the échelle diagram,  $\epsilon$  can be measured from the horizontal position of the  $l = 0$  ridge. In practice there is an ambiguity in  $\epsilon$  if  $n$  is not known (see Eq. 1.5). In the Sun we know from theoretical models that  $\epsilon \approx 1.5$  (rather than 0.5), which allows us to find the correct value of  $n$  for each mode. But it is important to remember that  $n$  is not directly observable.

### 1.2.5 Departures from the asymptotic relation

The asymptotic relation in Eq. 1.5 is only an approximation. Looking at Fig. 1.2, we see that the ridges all curve in an ‘S’ shape that is particularly pronounced at low frequencies. We also see that the  $l = 0$  and  $l = 2$  ridges converge towards to top, as do the  $l = 1$  and  $l = 3$  ridges. How should we best describe these departures? One approach is to say that  $\Delta\nu$  is a function of both  $l$  and frequency. In fact, doing

this is sufficient to describe all of the features just mentioned. However, it is physically more sensible to say instead that the convergence of the ridges is due to changes of the various *small* separations with frequency. Indeed, a linear dependence of  $\delta\nu_{02}$  on frequency fits the solar data quite well (Elsworth et al., 1990), and has been adopted for other stars (White et al., 2011). If we allow the small separations to vary with frequency then there is no longer any need to allow  $\Delta\nu$  to be a function of  $l$ .

What about the overall S-shaped curvature? This can be described as a change of  $\Delta\nu$  with frequency, and this is often done. However, it seems physically more sensible to ascribe the curvature to variations with frequency of  $\epsilon$  (e.g., Gough, 1986; Pérez Hernández and Christensen-Dalsgaard, 1998; Roxburgh, 2010). This allows  $\Delta\nu$  to have a single value that is independent of both  $l$  and frequency. However, in practice if we are given a set of frequencies (either observed or calculated) then  $\Delta\nu$  and  $\epsilon$  must be measured together, preferably in the region centred on  $\nu_{\max}$ . As we see from the open symbols in Fig. 1.2, a small change in  $\Delta\nu$  translates to quite a large change in  $\epsilon$ . These issues are discussed in some detail by White et al. (2011).

### 1.3 Ground-based observations

We now review some of the observations of solar-like oscillations. More details and additional references can be found in various review articles (e.g., Brown and Gilliland, 1994; Heasley et al., 1996; Bedding and Kjeldsen, 2003; Christensen-Dalsgaard, 2004; Cunha et al., 2007; Bazot et al., 2008; Bedding and Kjeldsen, 2008; Aerts et al., 2008). Figure 1.3 is an HR diagram showing most of the stars mentioned below.

When global oscillations were discovered in the Sun, it was quickly realised that measuring similar oscillations in Sun-like stars would be tremendously valuable. Several unsuccessful attempts were made (e.g., Traub et al., 1978; Baliunas et al., 1981; Smith, 1982) and some detections were claimed over the next decade but a review by Kjeldsen and Bedding (1995) concluded that none were convincing. However, it now seems clear that the excess power in the F5 star Procyon reported by Brown et al. (1991) was indeed due to oscillations and should be recognised as the first such detection, although it took some time and more observations for the large separation (about  $55\mu\text{Hz}$ ) to be established (Mosser et al., 1998; Martić et al., 1999; Barban et al., 1999). Furthermore, even a multi-



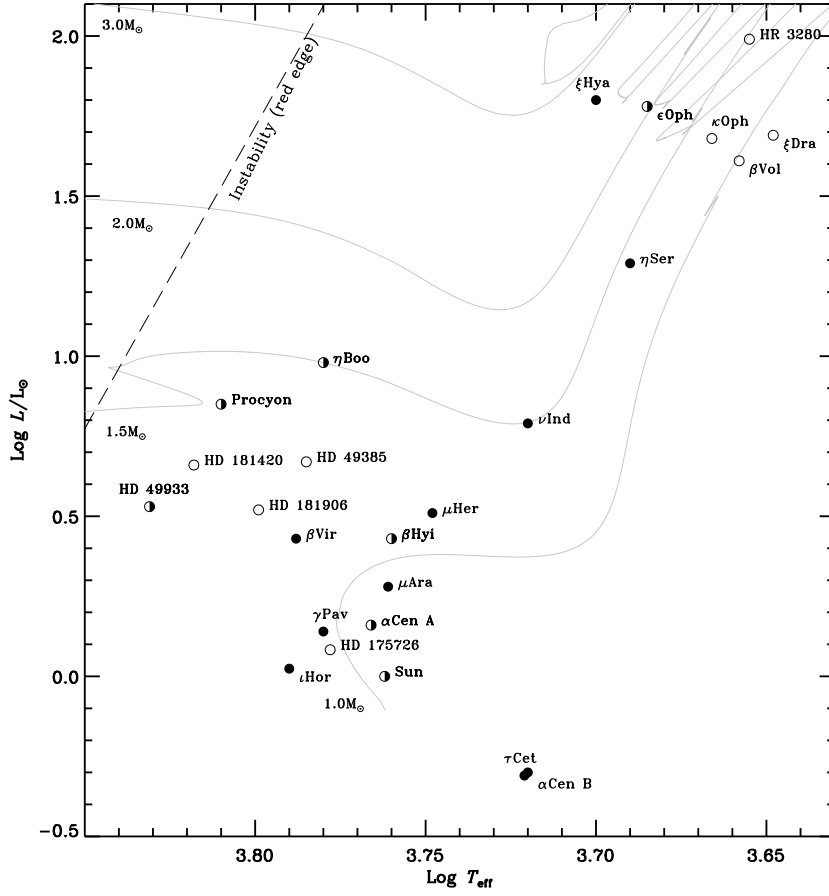


Figure 1.3 Hertzsprung-Russell diagram showing stars with solar-like oscillations for which  $\Delta\nu$  has been measured. Filled symbols indicate observations from ground-based spectroscopy and open symbols indicate space-based photometry (some stars were observed using both methods). Note that stars observed by *Kepler* are not included. Figure courtesy of Dennis Stello.

site campaign on Procyon using eleven telescopes at eight observatories (Arentoft et al., 2008) has failed to give an unambiguous mode identification (Bedding et al., 2010a), due to the short lifetimes of the oscillation modes (see Fig. 1.4). We refer to this as the F star problem (see also Sec. 1.4).

Most early oscillation searches measured Doppler shifts in radial velocities. However, a major effort to measure oscillations in intensity was

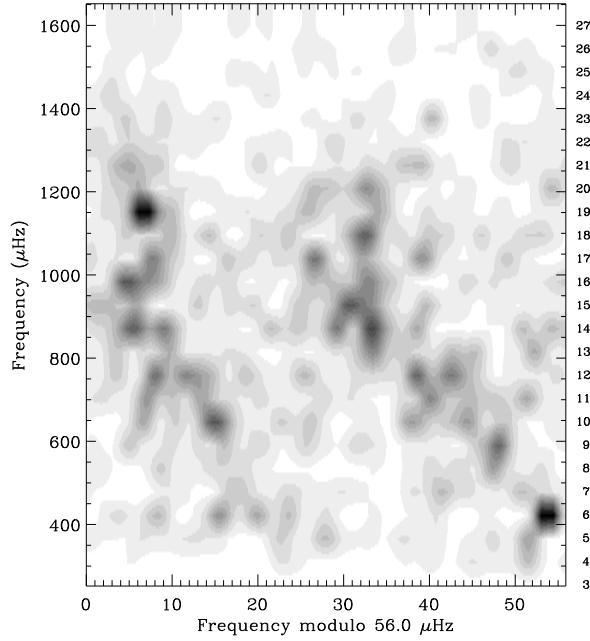


Figure 1.4 Échelle diagram of Procyon from the multi-site campaign, showing broadening due to short mode lifetimes (Bedding et al., 2010a). Which ridge is  $l = 1$  and which is  $l = 0$  and 2? Note that the power spectrum has been smoothed to a resolution of  $2 \mu\text{Hz}$ .

made in a multi-site photometric campaign on the open cluster M67 by Gilliland et al. (1993). Photometric measurements have the big advantage of allowing simultaneous measurements of many stars. This has now been done from space by the *CoRoT* and *Kepler* missions, but ground-based photometry is severely hampered by atmospheric scintillation. The Gilliland et al. (1993) M67 campaign did not produce definite detections, although it did indicate that oscillation amplitudes of F stars have lower amplitudes than expected from theoretical calculations (Kjeldsen and Bedding, 1995). It now seems clear that low oscillation amplitudes in F stars are a direct result of the short mode lifetimes that were mentioned above for Procyon.

A third method for detecting oscillations was applied by Kjeldsen et al. (1995) to the G0 subgiant  $\eta$  Boo. This method involved measuring fluctuations in the equivalent widths of the temperature-sensitive Balmer lines using low-resolution spectroscopy (see also Bedding et al., 1996). It produced good evidence for multiple oscillation modes in  $\eta$  Boo with

a large spacing of  $40 \mu\text{Hz}$ . Subsequent observations confirmed this result (Kjeldsen et al., 2003; Carrier et al., 2005), establishing  $\eta$  Boo as the first star apart from the Sun with a clear detection of solar-like oscillations. A very interesting result for  $\eta$  Boo, already apparent from the data obtained by Kjeldsen et al. (1995), was the departure of some of the dipole ( $l = 1$ ) modes from their regular spacing. This was interpreted by Christensen-Dalsgaard et al. (1995) as arising from bumping of mixed modes, as discussed in more detail in Sec. 1.8. Meanwhile, the equivalent-width method for observing oscillations turned out to be more sensitive to instrumental drifts than we hoped, although observations of  $\alpha$  Cen A did produce tentative evidence for p modes (Kjeldsen et al., 1999).

Major breakthroughs came from improvements in Doppler precision that were driven by the push to find extra-solar planets. Observations of the G2 subgiant star  $\beta$  Hyi, made with UCLES on the 3.9-m Anglo-Australian Telescope (Bedding et al., 2001) and confirmed with CORALIE on the 1.2-m Swiss Telescope (Carrier et al., 2001), showed a clear power excess with a regular spacing ( $\Delta\nu = 56 \mu\text{Hz}$ ). This result was hailed by Gough (2001) as the birth of asteroseismology, but that honour should probably go to the clear detection using CORALIE of the p-mode oscillation spectrum in  $\alpha$  Cen A by Bouchy and Carrier (2001, 2002) (Fig. 1.5).

Following on from these successes, a series of observations were made using high-resolution spectrographs on medium-to-large telescopes. Some spectrographs were equipped with an iodine cell, such as UCLES at the AAT (see above), UVES on the 8.2-m Very Large Telescope (e.g., Butler et al., 2004) and SARG on the 3.6-m Telescopio Nazionale Galileo (e.g., Bonanno et al., 2008). Other spectrographs used a thorium-argon lamp, including CORALIE (see above), as well as HARPS on the European Southern Observatory's 3.6-m telescope. HARPS has produced some particularly impressive results, including the first application of asteroseismology to a planet-hosting star ( $\mu$  Ara; see Bouchy et al. 2005; Bazot et al. 2005), an age for  $i$  Hor that implies it is an evaporated member of the primordial Hyades cluster (Vauclair et al., 2008), and the detection of oscillations in the remarkable solar twin 18 Sco (Bazot et al., 2011).

Another important development was the clear detection of oscillations in the red giant star  $\xi$  Hya based on one month of observations with CORALIE (Frandsen et al., 2002). This confirmed that red giants do indeed show solar-like oscillations, as already suspected from earlier observations of Arcturus and other stars. However, the oscillation peri-

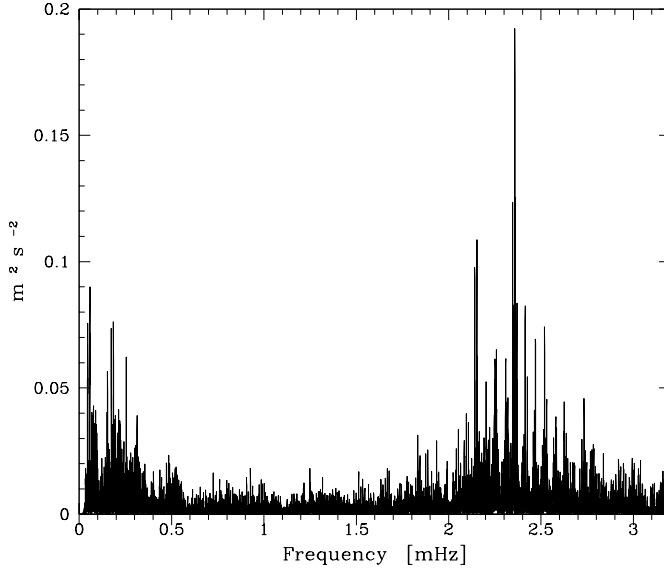


Figure 1.5 Power spectrum of  $\alpha$  Cen A from velocity observations over 13 night with the CORALIE spectrograph by Bouchy and Carrier (2002).

ods of several hours mean that extremely long time series are needed, and the development of red-giant asteroseismology had to wait until dedicated space missions, as discussed in Sec. 1.4.

Single-site observations suffer from aliases, which complicate the interpretation of the frequency spectrum (see Sec. 1.5). Some stars have been observed from two sites, including  $\zeta$  Her (Bertaux et al., 2003), Procyon (Martić et al., 2004; Kambe et al., 2008),  $\alpha$  Cen A (Bedding et al., 2004),  $\alpha$  Cen B (Kjeldsen et al., 2005),  $\nu$  Ind (a metal-poor subgiant; Bedding et al., 2006; Carrier et al., 2007), and  $\beta$  Hyi (Bedding et al., 2007). The star  $\beta$  Hyi is a subgiant that, like  $\eta$  Boo, shows mixed  $l = 1$  modes that are irregularly spaced (see Sec. 1.8).

Organising multi-site spectroscopic campaigns is difficult and the only example so far was carried out on Procyon (see above). The next step is SONG, a dedicated network of 1-m telescopes equipped with iodine-stabilized spectrographs Grundahl et al. (2006). The first node is currently under construction on Tenerife. Even in the era of space asteroseismology, ground-based velocity measurements retain some advantages. The background noise from stellar granulation is lower than for

intensity observations, allowing better signal-to-noise at low frequencies. There is also the ability to cover the whole sky and to target nearby stars whose parallaxes and other parameters are accurately known, such as the stars mentioned in this section.

## 1.4 Space-based observations

Making photometric measurements from space avoids the scintillation caused by the Earth's atmosphere and allows very high precision, even with a small telescope. Depending on the spacecraft orbit, it is possible to obtain long time series with few interruptions. The first space photometer dedicated to asteroseismology was the *EVRIS* experiment aboard the Russian *Mars 96* spacecraft. *EVRIS* was intended to carry out asteroseismology of bright stars during the cruise phase of the mission (Baglin, 1991; Buey et al., 1997) but unfortunately the launch failed and the mission was lost.

Other asteroseismology missions were proposed, including *PRISMA* (Appourchaux et al., 1993), *STARS* (Fridlund et al., 1994), *MONS* (Kjeldsen et al., 2000) and *Eddington* (Roxburgh and Favata, 2003). None of these made it though to construction and the first success came from an unexpected direction. After the failure of NASA's *Wide-Field Infrared Explorer* satellite (*WIRE*) immediately after launch due to the loss of coolant, its 50-mm star camera was used for asteroseismology by Buzasi (2002). *WIRE* was able to detect solar-like oscillations in  $\alpha$  Cen A (Schou and Buzasi, 2001; Fletcher et al., 2006) and also in several red giants (Buzasi et al., 2000; Retter et al., 2003; Stello et al., 2008). The SMEI experiment (Solar Mass Ejection Imager) on board the *Coriolis* satellite has also been used to measure oscillations in bright red giants (Tarrant et al., 2007, 2008). Finally, we note that the *Hubble Space Telescope* has been used on several occasions to observe solar-like oscillations, both via direct imaging (Edmonds and Gilliland, 1996; Gilliland, 2008; Stello and Gilliland, 2009) and also using its Fine Guidance Sensors (Zwintz et al., 1999; Kallinger et al., 2005; Gilliland et al., 2011).

The first dedicated asteroseismology mission to be launched successfully was *MOST* (*Microvariability and Oscillations of Stars*), which is a 15-cm telescope in low-Earth orbit (Walker et al., 2003). It has achieved great success with observations of classical (heat-engine) pulsators. In the realm of solar-like oscillations, controversy was generated when *MOST* failed to find evidence for oscillations in Procyon

(Matthews et al., 2004). However, Bedding et al. (2005) argued that the *MOST* non-detection was consistent with the ground-based data. Using photometry with *WIRE*, Bruntt et al. (2005) extracted parameters for the stellar granulation and found evidence for an excess due to oscillations. The discrepancy was finally laid to rest when Huber et al. (2011a) found an oscillation signal in a new and more accurate set of Procyon *MOST* data that agreed well with results from the ground-based velocity campaign (see Sec. 1.3).

The French-led *CoRoT* mission, launched in December 2006, is a 27-cm telescope in low-Earth orbit. It has contributed substantially to the list of main-sequence and subgiant stars with solar-like oscillations (e.g., Appourchaux et al., 2008; Michel et al., 2008; Barban et al., 2009; García et al., 2009; Mosser et al., 2009; Deheuvels et al., 2010; Mathur et al., 2010a). In particular, it has highlighted what might be called ‘the F star problem’ in stars such as HD 49933 (e.g., Appourchaux et al., 2008; Benomar et al., 2009), which is also a problem in Procyon (Bedding et al. 2010a; see also Bedding and Kjeldsen 2010). This refers to stars in which the mode lifetimes are so short that the  $l = 0$  and  $l = 2$  modes are blended, making them indistinguishable from  $l = 1$  modes. This makes it difficult to decide which ridge in the échelle diagram belongs to  $l = 1$  and which belongs to  $l = 0$  and 2, although measurement of  $\epsilon$  may be able to resolve this ambiguity (see Sec. 1.7).

A major achievement by *CoRoT* came from observations of hundreds G- and K-type red giants that showed clear oscillation spectra that were remarkably solar-like, with both radial and non-radial modes (De Ridder et al., 2009; Hekker et al., 2009; Carrier et al., 2010). *CoRoT* continues to produce excellent results on red giants (e.g., Miglio et al., 2009; Kallinger et al., 2010b; Mosser et al., 2010, 2011b), and also on main-sequence and subgiant stars (e.g., Mathur et al., 2010b; Ballot et al., 2011).

Finally we come to *Kepler*, which began science observations in May 2009. It has a 95-cm aperture and operates in an Earth-trailing helio-centric orbit, allowing continuous observations without interference from reflected light from the Earth. Although its primary goal is to search for extra-solar planets (Borucki et al., 2010), it is no exaggeration to say that *Kepler* is revolutionising asteroseismology (Gilliland et al., 2010b). Most stars are observed in long-cadence mode (sampling 29.4 minutes; see Jenkins et al. 2010), which is adequate to study oscillations in most red giants but is not fast enough for Sun-like stars. Fortunately, about

500 stars at a time can be observed in short-cadence mode (sampling 58.8 s; see Gilliland et al. 2010a).

For the first seven months of science operations, a survey was carried out with *Kepler's* short-cadence mode that targeted more than 2000 main-sequence and subgiant stars for one month each. The survey detected solar-like oscillations, including a clear measurement of  $\Delta\nu$ , for about 500 stars (Chaplin et al., 2011), representing an increase by a factor of  $\sim 20$  over the situation prior to *Kepler*.

Some of these stars have been studied individually. The first three to be published (Chaplin et al., 2010) were ‘Java’ (KIC 3656476), ‘Saxo’ (KIC 6603624) and ‘Gemma’ (KIC 11026764).<sup>2</sup> Java and Saxo are main-sequence stars, while Gemma is a subgiant showing bumped  $l = 1$  modes (Metcalfe et al. 2010; see Sec. 1.8 for a discussion of mode bumping). A small fraction of the survey stars were observed continuously since the start of the mission<sup>3</sup>. Of these, results have so far been published on ‘Tigger’ (KIC 11234888) and ‘Boogie’ (KIC 11395018) by Mathur et al. (2011), and on ‘Mulder’ (KIC 10273246) ‘Scully’ (KIC 10920273) by Campante et al. (2011).

As mentioned, the long-cadence mode of *Kepler* is perfectly adequate for red giants, and solar-like oscillations have been detected in thousands of them (e.g., Bedding et al., 2010b; Huber et al., 2010; Kallinger et al., 2010a; Hekker et al., 2011b), including some in open clusters (Stello et al., 2010; Basu et al., 2011; Hekker et al., 2011a). Some of these results are discussed in more detail in Sec. 1.9 (see also reviews by Hekker 2010 and Christensen-Dalsgaard 2011).

## 1.5 A few comments about Fourier analysis

Fourier analysis is an indispensable tool for asteroseismology. This section introduces some of the most important aspects. For more details including full references see, for example, Pijpers (2006), Aerts et al. (2010) and Appourchaux (2011).

The *amplitude spectrum* of a time series tells us which frequencies are

<sup>2</sup> Within the *Kepler* working groups, some stars are known by nicknames for convenience.

<sup>3</sup> Note that one of the 22 CCD modules on *Kepler* failed after seven months of operation. Since the spacecraft rotates by 90 degrees every three months to maintain the orientation of the solar panels, about 20% of stars will fall on this failed module at some time during the year, creating annual 3-month gaps in the data for those stars.

present, and with which amplitudes. Note that the *power spectrum* is simply the square of the amplitude spectrum. A useful way of thinking about the amplitude spectrum is as follows. We choose a frequency  $\nu$  and perform a least-squares fit of a sine wave to the time series. That is, we fix the frequency of the sine wave to be  $\nu$  and we vary the amplitude and phase until we get the best fit. If the quality of the time series is not uniform, as always happens with ground-based observations, it is important to weight the data using the measurement uncertainties (e.g., Frandsen et al., 1995). The amplitude of this best-fitting sine wave is our result (for solar-like oscillations, which are stochastically excited, we are usually not interested in the phase). Repeating this calculation for a range of different frequencies generates the amplitude spectrum.

This way of describing the amplitude spectrum allows us to understand several important properties. Firstly, it is clear that the observations do not need to be equally spaced in time (and ground-based observations generally are not). Now suppose our time series consists of a single sinusoidal signal. If we choose the correct frequency then the best-fitting amplitude will match the amplitude of the signal. If we choose completely the wrong frequency, the best-fitting sine wave will have a very small amplitude. But if we choose a frequency that is only slightly different from that of the signal, the best-fitting amplitude will be slightly less than the signal amplitude. Repeating this in small frequency steps will trace a sinc function ( $\sin \nu / \nu$ ). Increasing the length of the time series will decrease the width of this sinc function.

If there are regular gaps in the time series, as occurs for ground-based single-site observations, then choosing the wrong frequency will still give a significant response in some cases. For example, suppose the sine wave we are fitting has a higher frequency than the signal, such that exactly one extra cycle fits into the gap. This sine wave will still give a fairly good fit to the data and we will get an extra peak in the amplitude spectrum, called a *sidelobe*. The same thing occurs if the chosen frequency is exactly one cycle-per-gap *lower* than the signal frequency. We therefore expect two sidelobes, one on either side of the true peak. Sidelobes are an example of *aliasing*, which occurs when two or more different sine waves give good fits to the same data. The heights of the sidelobes relative to the true peak will decrease as the gaps get smaller (and the duty cycle improves). If the period of the gaps in the time series is  $T_{\text{gap}}$  then the sidelobes of a signal having frequency  $\nu$  will occur at frequencies of  $\nu \pm 1/T_{\text{gap}}$ . There will also be a smaller pair of peaks separated from the true peak by  $\nu \pm 2/T_{\text{gap}}$ , another pair at  $\nu \pm 3/T_{\text{gap}}$ , and so on.



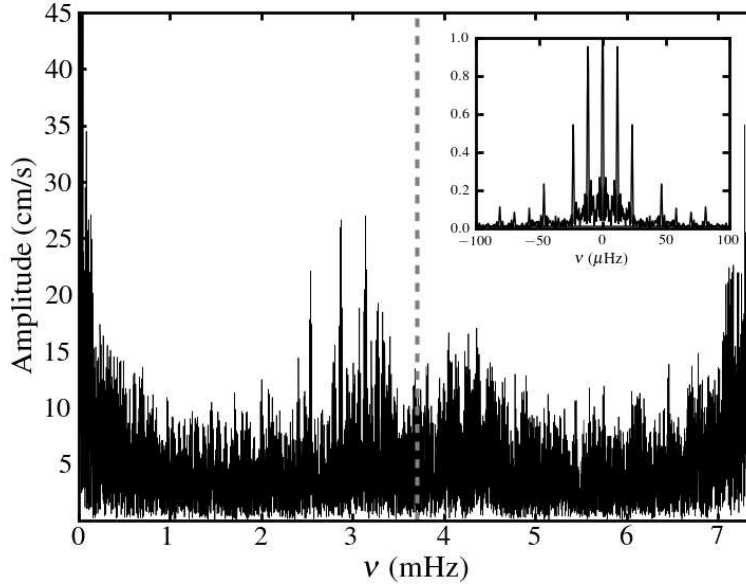


Figure 1.6 Amplitude spectrum of the solar twin 18 Sco, based on observations taken with HARPS over 12 nights. The inset shows the spectral window in amplitude, and the vertical dashed line shows the effective Nyquist frequency. Figure from Bazot et al. (2011).

This leads to the concept of the *spectral window*, which is the power spectrum of a pure sine wave. It is sometimes incorrectly called the *window function*, but that term actually refers to the sampling in the time domain. In practice, the spectral window should be calculated by averaging the power spectra of a sine and a cosine wave, to eliminate end effects. Note that this averaging should be done in power and not in amplitude. The inset of Fig. 1.6 shows an example.

Another example of aliasing occurs if the observations are regularly sampled. A single sine wave with frequency  $\nu$  that is sampled regularly at intervals separated by  $\delta t$  can be fitted equally well by a much higher-frequency sine wave having frequency  $2\nu_{\text{Nyq}} - \nu$ , where  $\nu_{\text{Nyq}} = 1/(2\delta t)$  is called the Nyquist frequency. This aliasing still occurs, although with reduced amplitude, if the sampling is not exactly regular. An example is shown in Fig. 1.6 for ground-based data. In this case, one can define an effective Nyquist frequency based on the median sampling.

It is sometimes assumed that the power spectrum does not contain any useful information above the Nyquist frequency, and that any signal

whose frequency is higher than  $\nu_{\text{Nyq}}$  cannot be measured. This is not true. For example, observations taken with *Kepler* in its long-cadence mode (sampling 29.4 minutes,  $\nu_{\text{Nyq}} = 283 \mu\text{Hz}$ ) still contain useful information about oscillations at higher frequencies, provided the power spectrum is interpreted with care.

### 1.6 Scaling relations for $\Delta\nu$ and $\nu_{\text{max}}$

As mentioned in Sec. 1.2.4, the large separation scales approximately with the square root of the mean stellar density:

$$\frac{\Delta\nu}{\Delta\nu_{\odot}} \approx \sqrt{\frac{\rho}{\rho_{\odot}}} = \left(\frac{M}{M_{\odot}}\right)^{0.5} \left(\frac{T_{\text{eff}}}{T_{\text{eff}\odot}}\right)^3 \left(\frac{L}{L_{\odot}}\right)^{-0.75}. \quad (1.6)$$

This scaling relation is very widely used, but how accurate is it? It was recently tested using theoretical models by White et al. (2011). Of course, given the curvature in the échelle diagram, the measurement of  $\Delta\nu$  depends on the frequency at which it is measured (see Sec. 1.2.4). The approach adopted by White et al. (2011) was to fit to the radial modes near  $\nu_{\text{max}}$  (see the paper for details). They confirmed generally good agreement with Eq. 1.6 but found departures reaching several percent. Interestingly, they found that these departures are predominantly a function of effective temperature and suggested a revised scaling relation that takes this into account.

Even if Equation 1.6 (or a modified version) agrees with theoretical models, this does not necessarily mean it is accurate for real stars. There are well-known discrepancies between the observed and calculated oscillation frequencies in the Sun, which are due to incorrect modeling of the surface layers (Christensen-Dalsgaard et al., 1988; Dziembowski et al., 1988; Rosenthal et al., 1999; Li et al., 2002). These discrepancies increase with frequency so there must also be a discrepancy in  $\Delta\nu$ . Indeed, the value of  $\Delta\nu$  of the best-fitting solar model is about 1% greater than the observed value (Kjeldsen et al., 2008). We can hardly expect the situation to be better in other stars, and a solution to the problem of modelling near-surface layers is urgently needed.

Another important and widely used scaling relation expresses  $\nu_{\text{max}}$  in terms of stellar parameters. It is based on the suggestion by Brown et al. (1991) that  $\nu_{\text{max}}$  might be expected to be a fixed fraction of the acoustic

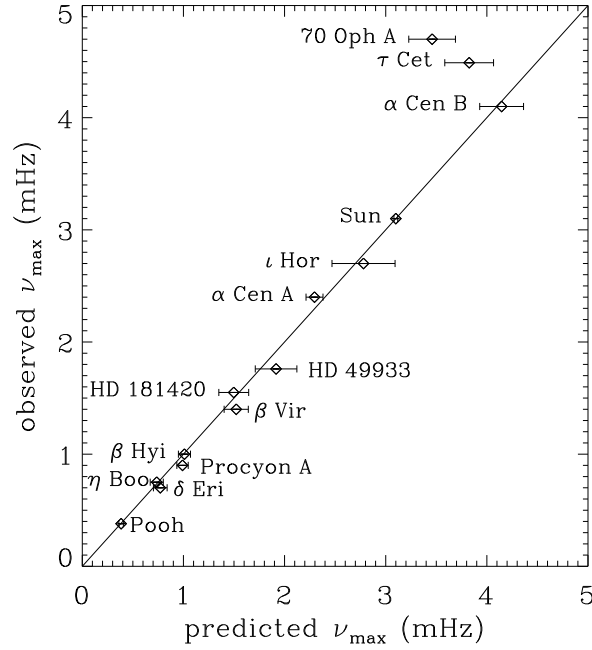


Figure 1.7 Testing the scaling relation for  $\nu_{\max}$ . Values for the stellar parameters were taken from the compilations by Bruntt (2009) and Bruntt et al. (2010), with the addition of ‘Pooh’ (KIC 4351319), a low-luminosity red giant observed by *Kepler* (Di Mauro et al., 2011).

cutoff frequency, which in turn scales as  $T_{\text{eff}}/\sqrt{g}$ . Hence we have:

$$\frac{\nu_{\max}}{\nu_{\max,\odot}} \approx \frac{M}{M_{\odot}} \left( \frac{T_{\text{eff}}}{T_{\text{eff},\odot}} \right)^{3.5} \left( \frac{L}{L_{\odot}} \right)^{-1}. \quad (1.7)$$

This relation has been shown to agree quite well with observations (Bedding and Kjeldsen, 2003) and also with model calculations (Chaplin et al., 2008b), and has recently been given some theoretical justification by Belkacem et al. (2011). Figure 1.7 shows the expected and observed values of  $\nu_{\max}$  for some well-studied stars with accurate parallaxes. There is generally very good agreement except for the two low-mass stars  $\tau$  Cet and 70 Oph A. If confirmed, this may indicate a breakdown of the assumption that  $\nu_{\max}$  is a fixed fraction of the acoustic cutoff frequency.

### 1.7 Ensemble asteroseismology

The wealth of data from *CoRoT* and *Kepler* allow us to carry out what might be called *ensemble asteroseismology*. This involves studying similarities and differences in groups of stars, and is complementary to the detailed study of a few individuals. Several groups have developed pipelines to process the large amounts of data and extract the global parameters such as  $\nu_{\max}$ ,  $\Delta\nu$  and amplitude. These various pipelines have been tested and compared using both simulations (Chaplin et al., 2008a) and *Kepler* data (Hekker et al., 2011c; Verner et al., 2011).

Ensemble asteroseismology can be carried out using asteroseismic diagrams, in which two properties of the oscillation spectra are plotted against one another. Here, we briefly discuss some of these diagrams.

**The C-D diagram:** The plot of small versus large frequency separations, first introduced by Christensen-Dalsgaard (1984), has come to be known as the C-D diagram. A modern version is shown in Fig. 1.8. In main-sequence stars, the tracks for different masses and ages are well spread, allowing both to be read off the diagram. However, note that the positions of the tracks depend on metallicity, and so this must be taken into account (for details and references, see White et al., 2011). For more evolved stars, the tracks converge and the small separation becomes much less sensitive as a diagnostic. C-D diagrams for red giants observed with *Kepler* have been presented by Bedding et al. (2010b) and Huber et al. (2010).

**The  $\nu_{\max}$ - $\Delta\nu$  diagram:** The strong correlation between  $\nu_{\max}$  and  $\Delta\nu$  was first plotted for main-sequence and subgiant stars by Stello et al. (2009) and for red giants by Hekker et al. (2009). The tightness of this relationship follows from the scaling relations (Eqs. 1.6 and 1.7), as discussed in some detail by Stello et al. (2009). The relationship extends over several orders of magnitude (see Fig. 1.9), making it a useful predictor of  $\Delta\nu$ .

**The  $\epsilon$  diagram:** As discussed in Sec. 1.2.4, the parameter  $\epsilon$  is sensitive to the surface layers of the star but needs to be measured carefully. A diagram showing  $\epsilon$  versus  $\Delta\nu$  was calculated by Christensen-Dalsgaard (1984), but its diagnostic potential was not realised until recently. Bedding and Kjeldsen (2010) suggested that  $\epsilon$  could be used as an aid to mode identification (the ‘F star problem’; see Secs. 1.3 and 1.4). The first observational  $\epsilon$

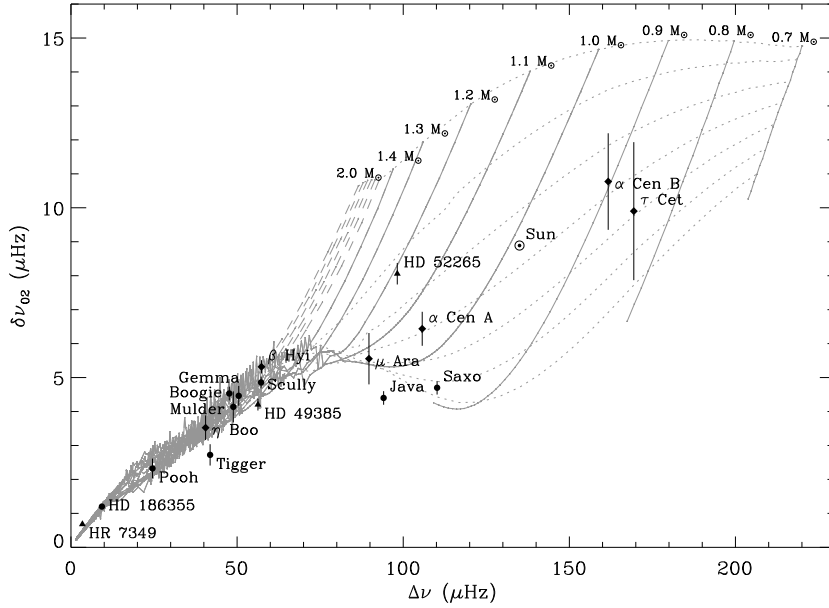


Figure 1.8 The so-called C-D diagram, which plots the large and small frequency separations. The solid lines show model calculations for solar metallicity using ASTEC and ADIPLS (Christensen-Dalsgaard, 2008a,b), with the dashed lines being isochrones from zero to 12 Gyr (top to bottom) in steps of 2 Gyr. The points show measurements of stars showing solar-like oscillations. Figure adapted from White et al. (2011).

diagram was made for red giants observed with *Kepler* by Huber et al. (2010), who used it to suggest mode identifications for four *CoRoT* red giants discussed by Hekker et al. (2010). Meanwhile, White et al. (2011) have shown that  $\epsilon$  is mostly determined by the stellar effective temperature and demonstrated that it is indeed useful for addressing the F star problem.

## 1.8 Mode bumping and avoided crossings

As mentioned in Sec. 1.2.1, mixed modes have p-mode character in the envelope and g-mode character in the core. They occur in evolved stars (subgiants and red giants), in which the large density gradient outside the core effectively divides the star into two coupled cavities. This leads to the phenomenon of *mode bumping*, in which mode fre-

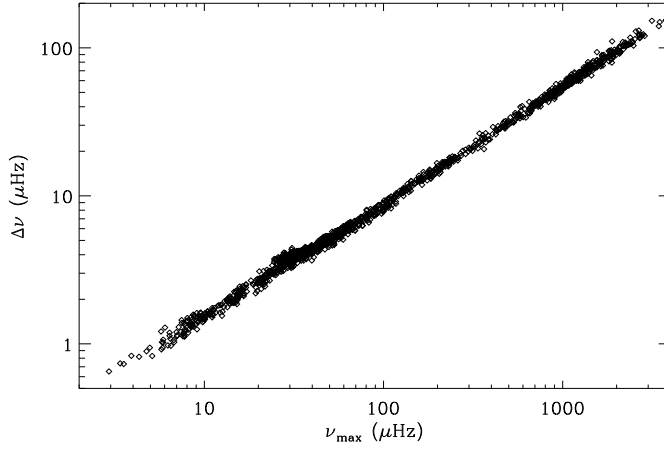


Figure 1.9 The strong correlation between  $\nu_{\max}$  and  $\Delta\nu$ , based on *Kepler* observations from the main sequence (upper right) to the red giants (lower left). Figure adapted from Huber et al. (2011b).

quencies are shifted from their regular spacing. Here, we summarise the main features of mixed modes from an observational perspective, which necessarily includes a basic introduction to the theory. For more details on the theoretical aspects see, for example, Scuflaire (1974); Osaki (1975); Aizenman et al. (1977); Dziembowski and Pamyatnykh (1991); Christensen-Dalsgaard (2004); Miglio et al. (2008); Dupret et al. (2009); Aerts et al. (2010).

Figure 1.10 shows theoretical oscillations frequencies for a subgiant star whose parameters were chosen to match  $\eta$  Boo. The left panel shows the evolution with time of the model frequencies for modes with  $l = 0$  (dashed lines) and  $l = 1$  (solid lines). The  $l = 0$  frequencies decrease slowly with time as the star expands. At a given moment in time, such as that marked by the vertical line, the radial modes are regularly spaced in frequency, with a large separation of  $\Delta\nu \approx 40 \mu\text{Hz}$ . However, the behaviour of the  $l = 1$  modes (solid lines) is rather different. They undergo a series of *avoided crossings* (Osaki, 1975; Aizenman et al., 1977), during which an  $l = 1$  mode is bumped upwards by the mode below, and in turn it bumps the mode above. The effect is to disturb the regular spacing of the  $l = 1$  modes in the vicinity of each avoided crossing. The right panel of Fig. 1.10 shows the frequencies in échelle format for the single model that is marked in the left panel by the vertical line. The bumping from regularity of the  $l = 1$  modes (triangles) is obvious and

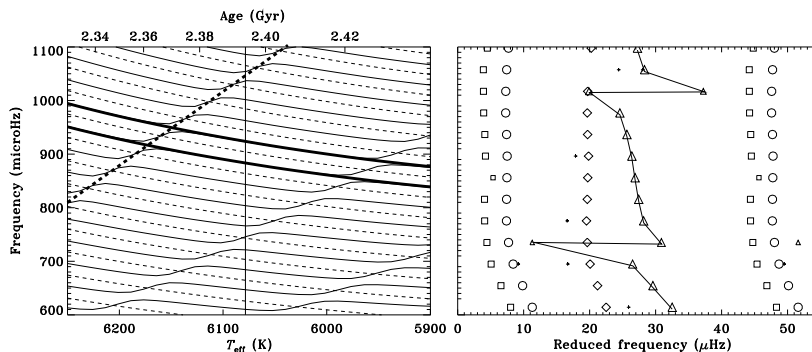


Figure 1.10 Left: Evolution of oscillation frequencies in models of a subgiant star of mass  $1.60M_{\odot}$  and  $Z = 0.03$  (representing  $\eta$  Boo). The dashed lines correspond to modes of degree  $l = 0$ , and the solid lines to  $l = 1$ . The vertical solid line indicates the location of the model whose frequencies are illustrated in the right panel, the thick solid lines show two of the  $l = 1$   $\pi$  modes and the thick dashed line shows one of the  $\gamma$  modes (see text). Right: Échelle diagram using a frequency separation of  $\Delta\nu = 40.3\mu\text{Hz}$  and a zero-point frequency of  $\nu_0 = 735\mu\text{Hz}$ . Circles are used for modes with  $l = 0$ , triangles for  $l = 1$ , squares for  $l = 2$  and diamonds for  $l = 3$ . The size of the symbols indicates the relative amplitude of the modes, estimated from the mode inertia, with crosses used for modes whose symbols would otherwise be too small. Figures adapted from Christensen-Dalsgaard et al. (1995).

there is one extra  $l = 1$  mode at each avoided crossing, where the modes are “squeezed together”.

Bumping of  $l = 1$  modes has been observed in the subgiant stars  $\eta$  Boo (Kjeldsen et al., 1995, 2003; Carrier et al., 2005),  $\beta$  Hyi (Bedding et al., 2007), the *CoRoT* target HD 49385 (Deheuvels et al., 2010) and the *Kepler* target ‘Gemma’ (KIC 11026764; Metcalfe et al. 2010). Many other subgiants stars observed with *Kepler* also show bumping of  $l = 1$  modes, and observations have so far been published for ‘Tigger’ (KIC 11234888) and ‘Boogie’ (KIC 11395018) by Mathur et al. (2011), and for ‘Mulder’ (KIC 10273246) and ‘Scully’ (KIC 10920273) by Campante et al. (2011). It was also suggested by Bedding et al. (2010a) that Procyon has an  $l = 1$  mixed mode at low frequency (see Fig. 1.4), based on the narrowness of the peak in the power spectrum. Note that mixed modes are expected to have longer lifetimes (smaller linewidths) than pure  $p$  modes because they have larger mode inertias (e.g., Christensen-Dalsgaard,

2004). Mode inertia is a measure of the total interior mass that is affected by the oscillation.

We now discuss the theoretical aspects of mixed modes in more detail. In particular, what causes the mode bumping and why are  $l = 1$  modes the most affected? To answer these questions, we return to the idea of a star with two cavities, as mentioned above. We can think of subgiants and red giants as having p modes trapped in the envelope and g modes trapped in the core. Strictly speaking, these are hypothetical modes within each cavity rather than true oscillation modes of the whole star, and so they should probably be called ‘envelope p modes’ and ‘core g modes’. Aizenman et al. (1977) referred to these artificially isolated modes as  $\pi$  modes and  $\gamma$  modes, which is a useful abbreviation that we will adopt. They are the modes that would exist if the two cavities were completely decoupled. In reality, there is coupling and this leads to a mixed mode whenever a  $\pi$  mode and a  $\gamma$  mode with the same  $l$  are sufficiently close to each other in frequency. This mixed mode has p-mode character in the envelope and g-mode character in the core. Note also that the frequencies of the  $\pi$  modes decrease with time as the star evolves, while those of the  $\gamma$  modes increase with time.

This picture allows to understand the features seen in Fig. 1.10. For  $l = 0$  there are no mixed modes because radial g modes do not exist and so we have pure p modes that are regularly spaced in frequency. For  $l = 1$ , the  $\gamma$  modes are visible as the three upward-sloping ridges, one of which is marked with a thick dashed line (see also Fig. 1b of Aizenman et al., 1977). The  $l = 1$   $\pi$  modes can also be traced in Fig. 1.10 by connecting the downward-sloping parts of the tracks, as shown for two adjacent  $\pi$  modes by the thick solid lines. Recall that a mixed mode occurs when a  $\pi$  mode and a  $\gamma$  mode are close to each other in frequency, which happens at the intersections. In fact, we see that several  $\pi$  modes are able to couple with each  $\gamma$  mode (see Deheuvels and Michel, 2010a). Indeed, all the  $l = 1$  modes are bumped to some extent, with those closest in frequency to each  $\gamma$  mode being bumped the most, as seen in the échelle diagram (right panel of Fig. 1.10).<sup>4</sup>

Figure 1.11 shows the situation for the  $l = 2$  modes in a similar set of models. The coupling between the two cavities for  $l = 2$  modes is much weaker than for  $l = 1$  modes,<sup>5</sup> which means that the  $\pi$  and  $\gamma$  modes must have almost exactly the same frequency in order to couple.

<sup>4</sup> “All modes are mixed, but some modes are more mixed than others” (with apologies to George Orwell, 1945).

<sup>5</sup> The coupling strength varies inversely with the width of the evanescent region



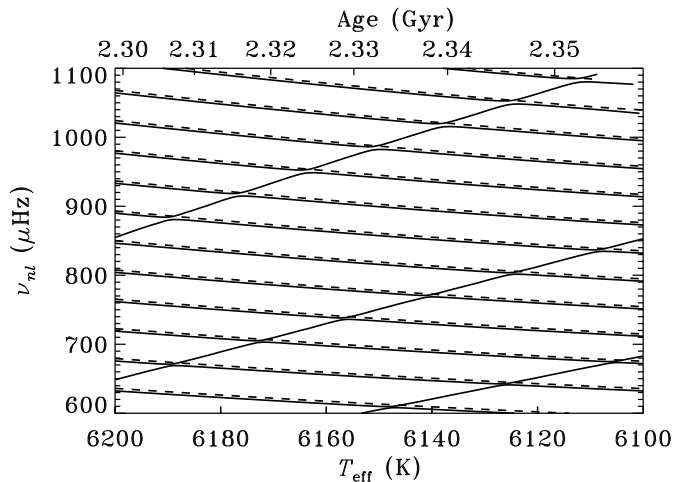


Figure 1.11 Avoided crossings for  $l = 2$  modes in a model of  $\eta$  Boo. This is similar to the left panel of Fig. 1.10, but for a slightly different model and with the solid lines now showing  $l = 2$  modes (the dashed lines again show  $l = 0$  modes). Adapted from Christensen-Dalsgaard and Houdek (2010).

In Fig. 1.11 we see that the  $l = 2$  modes (solid lines) mostly slope downward (following the  $\pi$ -mode tracks), indicating they are essentially behaving as pure p modes. The upward-sloping segments (which follow the  $\gamma$ -mode tracks) correspond to modes behaving essentially as pure g modes. These g-dominated modes will have very high inertias and very low amplitudes, making them undetectable. As a result, the observable  $l = 2$  modes will only be bumped slightly or not at all, as can be seen in the right panel of Fig. 1.10 (squares).

### 1.8.1 The p-g diagram

It has long been recognised that mixed modes have great potential for asteroseismology because their frequencies are very sensitive to stellar interiors and because they change quite rapidly as the star evolves (e.g., Dziembowski and Pamyatnykh, 1991; Christensen-Dalsgaard et al., 1995). One way to exploit this information is by performing a direct comparison of observed frequencies with models. This has been done for  $\eta$  Boo (Christensen-Dalsgaard et al., 1995; Guenther and Demarque, 1996; Di Mauro et al.,

between the two cavities, and this region turns out to be wider for  $l = 2$  modes than for  $l = 1$  modes (Christensen-Dalsgaard, 2004).

2003a; Guenther, 2004; Carrier et al., 2005),  $\beta$  Hyi (Di Mauro et al., 2003b; Fernandes and Monteiro, 2003; Brandão et al., 2011), the *CoRoT* target HD 49385 (Deheuvels and Michel, 2010a) and the *Kepler* target ‘Gemma’ (Metcalf et al., 2010).

However, adjusting the model parameters to fit the observed frequencies can be difficult and time-consuming. We can ask whether the information contained in the mixed modes can be used more elegantly. Based on the preceding discussion of mixed modes and mode bumping, we are led to consider the frequencies of the avoided crossings themselves. For example, the échelle diagram in Fig. 1.10 shows two avoided crossings<sup>6</sup>, at about 730 and 1050  $\mu\text{Hz}$ . We recognise these as the frequencies of the  $\gamma$  modes (recall that these are the pure g modes that would exist in the core cavity if it could be treated in isolation). Much of the diagnostic information contained in the mixed modes can be captured in this way. This is because the overall pattern of the mixed modes is determined by the mode bumping at each avoided crossing, and these patterns are determined by the g modes trapped in the core (the  $\gamma$  modes). For related discussion on this point, see Deheuvels and Michel (2010b).

This discussion suggests a new asteroseismic diagram, inspired by the classical C-D diagram, in which the frequencies of the avoided crossings (the  $\gamma$  modes) are plotted against the large separation of the p modes. This p-g diagram, so named because it plots g-mode frequencies versus p-mode frequencies, could prove to be an instructive way to display results of many stars and to make a first comparison with theoretical models (Campante et al. 2011; Bedding et al., in prep.).

## 1.9 Solar-like oscillations in red giants

As outlined in Sec. 1.4, there has recently been tremendous progress in asteroseismology of G- and K-type red giants, with solar-like oscillations detected by *CoRoT* and *Kepler* in thousands of stars. There have also been rapid developments in the theory (e.g., Guenther et al., 2000; Dziembowski et al., 2001; Christensen-Dalsgaard, 2004; Dupret et al., 2009; Montalbán et al., 2010; Di Mauro et al., 2011), as discussed in detail by Christensen-Dalsgaard (2011) in this volume.

<sup>6</sup> Strictly speaking, these features in the échelle diagram should not really be called avoided crossings, since that term refers to the close approaches of two modes in the evolution diagram. However, there does not seem to be any harm in using the term.

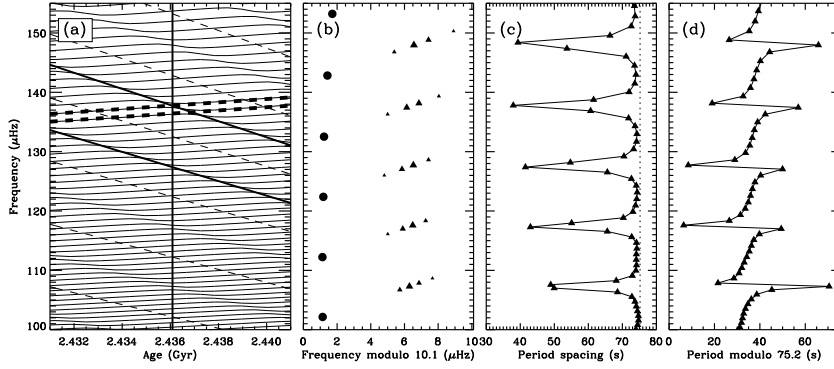


Figure 1.12

At first glance, the oscillation spectra of red giants are remarkably solar-like. As first revealed by *CoRoT* observations (De Ridder et al., 2009), they have radial and non-radial modes that closely follow the asymptotic relation. In fact, to a large extent their power spectra are simply scaled versions of each other, so that the large and small spacings are in a roughly constant ratio (e.g., Bedding et al., 2010b). This high degree of homology is rather unhelpful for asteroseismology, in the sense that the small separations lack much of the diagnostic potential that makes them so valuable in main-sequence stars. Fortunately, there are other features in the oscillation spectra of red giants that make up for this loss. We now discuss one of them in some detail, namely the presence of mixed modes with g-mode period spacings.

Even after the first month, *Kepler* data revealed multiple  $l = 1$  modes per order that indicated the presence of mixed modes (see Fig. 5 of Bedding et al., 2010b). As with the subgiants discussed in Sec. 1.8, the large density gradient outside the helium core divides the star into two coupled cavities, with the oscillations behaving like p modes in the envelope and like g modes in the core. The difference with red giants is that the spectrum of g modes in the core (the  $\gamma$  modes) is much denser. It is also important to note that, while p modes are approximately equally spaced in frequency (see Sec. 1.2.2), an asymptotic analysis shows that g modes are approximately equally spaced in *period* (Tassoul, 1980).

Figure 1.12a shows the time evolution of frequencies of a red giant model for modes with  $l = 0$  (dashed lines) and  $l = 1$  (solid lines). It is very instructive to compare this with Fig. 1.10. In both cases we can follow the downward-sloping  $l = 1$   $\pi$  modes (two examples are shown by

thick solid lines). They are approximately equally spaced in frequency (with separation  $\Delta\nu$ ) and they run parallel to the  $l = 0$  modes (which are pure p modes). In both figures we can also follow the upward-sloping  $l = 1$   $\gamma$  modes (examples shown by thick dashed lines). The difference is that for the subgiant in Fig. 1.10, there are only three  $\gamma$  modes, but for the red giant in Fig. 1.12a there are dozens. As before, we have a mixed mode for every  $\pi$  mode and a mixed mode for every  $\gamma$  mode. Most of these mixed modes are g-dominated (they follow the  $\gamma$ -mode tracks), with very high inertia and very low amplitude. However, some mixed modes fall close enough to a  $\pi$  mode for the coupling to be significant, producing p-dominated mixed modes with sufficient amplitude to be observable. These are shown by the triangles in Fig 1.12b, which is the échelle diagram of the model indicated by the vertical line in Fig. 1.12a. Note that the clusters of observed  $l = 1$  modes are centred at the positions expected for pure  $l = 1$  p modes, which are about half way between the  $l = 0$  modes.

The pattern of  $l = 1$  clusters described above has been observed in red giants using data from *Kepler* (Beck et al., 2011; Bedding et al., 2011) and *CoRoT* (Mosser et al., 2011a). The spacings within the  $l = 1$  clusters clearly provide valuable information about the gravity modes trapped in the core but to interpret them we must take into account the mode bumping. Each cluster is squeezed together by the presence of one extra mode and so the spacing we measure from the observable modes, which we denote  $\Delta P_{\text{obs}}$ , will be substantially less than the spacing of the core g modes (the  $\gamma$  modes), which we denote  $\Delta P_g$ . This is shown for the model in Fig. 1.12c, which plots the period spacing between consecutive  $l = 1$  mixed modes. From the upper envelope we see that  $\Delta P_g \approx 75$  s, but this is determined from the g-dominated modes, whereas the observable (p-dominated) modes have period differences that are lower by a factor ranging from 1.2 to 2.

Another way to visualise the frequencies is shown in Fig. 1.12d. This shows the model frequencies for  $l = 1$  in échelle format, but setting the horizontal axis to be period modulo the g-mode period spacing (rather than frequency modulo the large frequency separation). Doing this for real stars is difficult because most of the  $l = 1$  modes are not observable, so that finding the correct period spacing is equivalent to estimating the exact number of missing  $l = 1$  modes in each gap. Bedding et al. (2011) were only able to do this unambiguously for those stars with the largest number of detected modes. For the remainder, however, it was still possible to measure the average period spacing of the observed  $l = 1$

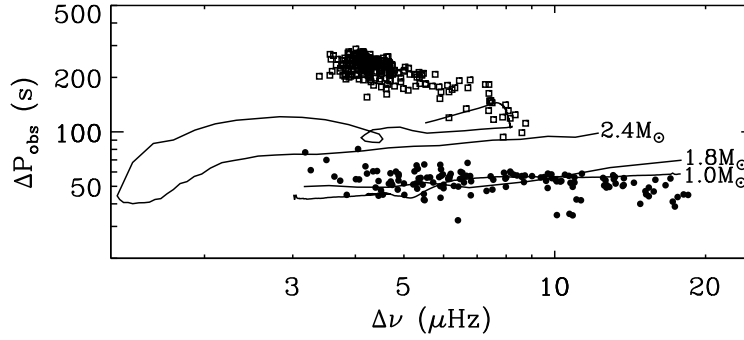


Figure 1.13 Period spacings of  $l = 1$  modes in red giants. The symbols are measurements obtained with *Kepler* (Bedding et al., 2011). Filled circles indicate hydrogen-shell-burning giants and open squares indicate helium-core-burning stars. The solid lines show model calculations using ASTEC and ADIPLS (Christensen-Dalsgaard, 2008a,b). The period spacings were computed from the models by averaging over the observable modes (see White et al., 2011, for details). The hydrogen-shell-burning giants evolve from right to left as they ascend the red giant branch. The  $2.4\text{-}M_{\odot}$  model continues into the helium-core-burning stage, looping back to the right to join the so-called secondary clump Girardi (1999). The lower-mass models stop before the helium-burning stage because they undergo a helium flash that cannot be calculated by ASTEC. Solar metallicity was adopted for all models, which were computed without mass loss.

modes ( $\Delta P_{\text{obs}}$ ). This quantity is plotted in Fig. 1.13 against the large frequency separation, and the stars are seen to divide nicely into two groups (see also Mosser et al., 2011a). Theoretical models confirm that these groups correspond to stars still burning hydrogen in a shell (filled circles) and those also burning helium in the core (open squares; for more details see Bedding et al. 2011; White et al. 2011). These issues are discussed in detail in this volume by Christensen-Dalsgaard (2011), who shows that the larger period spacing in He-burning stars is due to the presence of a convective core.

Finally, Simon O'Toole (priv. comm.) has pointed out that the close agreement between the period spacings found in the He-burning red giants with the those hot subdwarf B (sdB) stars from *Kepler* data (Reed et al., 2011) is nicely consistent with the accepted explanation that sdB stars are the cores of He-burning red giants that have lost their envelopes.

**Acknowledgments** Many thanks to Pere Pallé and colleagues for organising this fantastic Winter School. I am grateful to Dennis Stello, Tim White and Jørgen Christensen-Dalsgaard for providing figures. I also thank them, as well as Hans Kjeldsen, Daniel Huber and Othman Benomar, for many helpful discussions.

## References

- Aerts, C., Christensen-Dalsgaard, J., Cunha, M., & Kurtz, D. W. 2008. The Current Status of Asteroseismology. *Sol. Phys.*, **251**, 3.
- Aerts, C., Christensen-Dalsgaard, J., & Kurtz, D. W. 2010. *Asteroseismology*. Springer: Heidelberg.
- Aizenman, M., Smeyers, P., & Weigert, A. 1977. Avoided Crossing of Modes of Non-radial Stellar Oscillations. *A&A*, **58**, 41.
- Althaus, L. G., Córscico, A. H., Isern, J., & García-Berro, E. 2010. Evolutionary and pulsational properties of white dwarf stars. *A&A Rev.*, **18**, 471.
- Antoci, V., Handler, G., Campante, T. L., et al. 2011. Solar-like oscillations as probe of the convective envelope of a delta Scuti star. *Nature*. submitted.
- Appourchaux, T. 2011. A crash course on data analysis in asteroseismology. In: *this volume*.
- Appourchaux, T., Gough, D. O., Catala, C., et al. 1993. Prisma - the First Space Mission to See Inside the Stars. Page 411 of: Brown, T. M. (ed), *GONG 1992: Seismic Investigation of the Sun and Stars*, vol. 42. ASP Conf. Ser.
- Appourchaux, T., Michel, E., Auvergne, M., et al. 2008. CoRoT sounds the stars: p-mode parameters of Sun-like oscillations on HD 49933. *A&A*, **488**, 705.
- Arentoft, T., Kjeldsen, H., Bedding, T. R., et al. 2008. A multi-site campaign to measure solar-like oscillations in Procyon. I. Observations, Data Reduction and Slow Variations. *ApJ*, **687**, 1180.
- Baglin, A. 1991. Stellar seismology from space - The EVRIS experiment on board Mars 94. *Sol. Phys.*, **133**, 155.
- Baliunas, S. L., Vaughan, A. H., Hartmann, L., Liller, W., & Dupree, A. K. 1981. Short time-scale variability of chromospheric CA II in late-type stars. *ApJ*, **246**, 473.
- Ballot, J. 2010. Current methods for analyzing light curves of solar-like stars. *Astron. Nachr.*, **331**, 933.
- Ballot, J., Gizon, L., Samadi, R., et al. 2011. Accurate p-mode measurements of the G0V metal-rich CoRoT target HD 52265. *A&A*, **530**, A97.
- Balona, L. A., Pigulski, A., De Cat, P., et al. 2011. Kepler observations of the variability in B-type stars. *MNRAS*, **413**, 2403.

- Barban, C., Michel, E., Martić, M., et al. 1999. Solar-like oscillations of Procyon A: stellar models and time series simulations versus observations. *A&A*, **350**, 617.
- Barban, C., Deheuvels, S., Baudin, F., et al. 2009. Solar-like oscillations in HD 181420: data analysis of 156 days of CoRoT data. *A&A*, **506**, 51.
- Basu, S., Grundahl, F., Stello, D., et al. 2011. Sounding Open Clusters: Asteroseismic Constraints from Kepler on the Properties of NGC 6791 and NGC 6819. *ApJ (Letters)*, **729**, L10.
- Bazot, M., Vauclair, S., Bouchy, F., & Santos, N. C. 2005. Seismic analysis of the planet-hosting star  $\mu$  Arae. *A&A*, **440**, 615.
- Bazot, M., Monteiro, M. J. P. F. G., & Straka, C. W. 2008. Current Issues in Asteroseismology. Page 012008 of: Gizon, L. & Roth, M. (eds), *Second HELAS International Conference: Helioseismology, Asteroseismology and MHD Connections*, vol. 118. Journal of Physics Conference Series.
- Bazot, M., Ireland, M. J., Huber, D., et al. 2011. The radius and mass of the close solar twin 18 Scorpii derived from asteroseismology and interferometry. *A&A*, **526**, L4.
- Beck, P. G., Bedding, T. R., Mosser, B., et al. 2011. Kepler Detected Gravity-Mode Period Spacings in a Red Giant Star. *Science*, **332**, 205.
- Bedding, T. R. 2003. Solar-like oscillations in semiregular variables. *Ap&SS*, **284**, 61.
- Bedding, T. R. & Kjeldsen, H. 2003. Solar-like oscillations. *PASA*, **20**, 203.
- Bedding, T. R. & Kjeldsen, H. 2008. Asteroseismology from solar-like oscillations. Page 21 of: *14th Cambridge Workshop on Cool Stars, Stellar Systems, and the Sun*, vol. 384. ASP Conf. Ser.
- Bedding, T. R. & Kjeldsen, H. 2010. Scaled oscillation frequencies and échelle diagrams as a tool for comparative asteroseismology. *Commun. Asteroseismology*, **161**, 3.
- Bedding, T. R., Kjeldsen, H., Reetz, J., & Barbuy, B. 1996. Measuring stellar oscillations using equivalent widths of absorption lines. *MNRAS*, **280**, 1155.
- Bedding, T. R., Butler, R. P., Kjeldsen, H., et al. 2001. Evidence for solar-like oscillations in  $\beta$  Hydri. *ApJ*, **549**, L105.
- Bedding, T. R., Kjeldsen, H., Butler, R. P., et al. 2004. Oscillation frequencies and mode lifetimes in  $\alpha$  Centauri A. *ApJ*, **614**, 380.
- Bedding, T. R., Kjeldsen, H., Bouchy, F., et al. 2005. The non-detection of oscillations in Procyon by MOST: Is it really a surprise? *A&A*, **432**, L43.
- Bedding, T. R., Butler, R. P., Carrier, F., et al. 2006. Solar-like oscillations in the metal-poor subgiant  $\nu$  Indi: constraining the mass and age using asteroseismology. *ApJ*, **647**, 558.
- Bedding, T. R., Kjeldsen, H., Arentoft, T., et al. 2007. Solar-like oscillations in the G2 subgiant  $\beta$  Hydri from dual-site observations. *ApJ*, **663**, 1315.
- Bedding, T. R., Kjeldsen, H., Campante, T. L., et al. 2010a. A multi-site campaign to measure solar-like oscillations in Procyon. II. Mode Frequencies. *ApJ*, **713**, 935.



- Bedding, T. R., Huber, D., Stello, D., et al. 2010b. Solar-like Oscillations in Low-luminosity Red Giants: First Results from Kepler. *ApJ (Letters)*, **713**, L176.
- Bedding, T. R., Mosser, B., Huber, D., et al. 2011. Gravity modes as a way to distinguish between hydrogen- and helium-burning red giant stars. *Nature*, **471**, 608.
- Belkacem, K., Samadi, R., Goupil, M.-J., et al. 2009. Solar-Like Oscillations in a Massive Star. *Science*, **324**, 1540.
- Belkacem, K., Dupret, M. A., & Noels, A. 2010. Solar-like oscillations in massive main-sequence stars. I. Asteroseismic signatures of the driving and damping regions. *A&A*, **510**, A6.
- Belkacem, K., Goupil, M. J., Dupret, M. A., et al. 2011. The underlying physical meaning of the  $\nu_{\max} - \nu_c$  relation. *A&A*. in press; arXiv:1104.0630.
- Benomar, O., Baudin, F., Campante, T. L., et al. 2009. A fresh look at the seismic spectrum of HD49933: analysis of 180 days of CoRoT photometry. *A&A*, **507**, L13.
- Bertaux, J.-L., Schmitt, J., Lebrun, J.-C., Bouchy, F., & Guibert, S. 2003. Two-site simultaneous observations of solar-like stellar oscillations in radial velocities with a Fabry-Pérot calibration system. *A&A*, **405**, 367.
- Bonanno, A., Benatti, S., Claudi, R., et al. 2008. Detection of Solar-like Oscillations in the G5 Subgiant  $\mu$  Her. *ApJ*, **676**, 1248.
- Borucki, W. J., Koch, D., Basri, G., et al. 2010. Kepler Planet-Detection Mission: Introduction and First Results. *Science*, **327**, 977.
- Bouchy, F. & Carrier, F. 2001. P-mode observations on  $\alpha$  Cen A. *A&A*, **374**, L5.
- Bouchy, F. & Carrier, F. 2002. The acoustic spectrum of alpha Cen A. *A&A*, **390**, 205.
- Bouchy, F., Bazot, M., Santos, N. C., Vauclair, S., & Sosnowska, D. 2005. Asteroseismology of the planet-hosting star  $\mu$  Arae. I. The acoustic spectrum. *A&A*, **440**, 609.
- Brandão, I. M., Doğan, G., Christensen-Dalsgaard, J., et al. 2011. Asteroseismic modelling of the solar-type subgiant star  $\beta$  Hydri. *A&A*, **527**, A37.
- Broomhall, A.-M., Chaplin, W. J., Davies, G. R., et al. 2009. Definitive Sun-as-a-star p-mode frequencies: 23 years of BiSON observations. *MNRAS*, **396**, L100.
- Brown, T. M. & Gilliland, R. L. 1994. Asteroseismology. *ARA&A*, **32**, 37.
- Brown, T. M., Gilliland, R. L., Noyes, R. W., & Ramsey, L. W. 1991. Detection of possible  $p$ -mode oscillations on Procyon. *ApJ*, **368**, 599.
- Bruntt, H. 2009. Accurate fundamental parameters of CoRoT asteroseismic targets. The solar-like stars HD 49933, HD 175726, HD 181420, and HD 181906. *A&A*, **506**, 235.
- Bruntt, H., Kjeldsen, H., Buzasi, D. L., & Bedding, T. R. 2005. Evidence for Granulation and Oscillations in Procyon from Photometry with the WIRE satellite. *ApJ*, **633**, 440.
- Bruntt, H., Bedding, T. R., Quirion, P.-O., et al. 2010. Accurate fundamental parameters for 23 bright solar-type stars. *MNRAS*, **405**, 1907.

- Buey, J. T., Auvergne, M., Vuillemin, A., & Epstein, G. 1997. Towards Asteroseismology from Space: the EVRIS Experiment. I. The Photometer: Description and Calibration. *PASP*, **109**, 140.
- Butler, R. P., Bedding, T. R., Kjeldsen, H., et al. 2004. Ultra-high-precision velocity measurements of oscillations in  $\alpha$  Cen A. *ApJ*, **600**, L75.
- Buzasi, D. L. 2002. Asteroseismic Results from WIRE. Page 616 of: Aerts, C., Bedding, T. R., & Christensen-Dalsgaard, J. (eds), *IAU Colloquium 185: Radial and Nonradial Pulsations as Probes of Stellar Physics*, vol. 259. ASP Conf. Ser.
- Buzasi, D. L., Catanzarite, J., Laher, R., et al. 2000. The detection of multimodal oscillations on  $\alpha$  Ursae Majoris. *ApJ*, **532**, L133.
- Campante, T. L., Handberg, R., Mathur, S., et al. 2011. Asteroseismology from *Kepler* ten-month time series: the evolved Sun-like stars KIC 10273246 and KIC 10920273. *A&A*. submitted.
- Cantiello, M., Langer, N., Brott, I., et al. 2009. Sub-surface convection zones in hot massive stars and their observable consequences. *A&A*, **499**, 279.
- Carrier, F., Bouchy, F., Kienzie, F., et al. 2001. Solar-like oscillations in  $\beta$  Hydri: Confirmation of a stellar origin for the excess power. *A&A*, **378**, 142.
- Carrier, F., Eggenberger, P., & Bouchy, F. 2005. New seismological results on the G0 IV  $\eta$  Bootis. *A&A*, **434**, 1085.
- Carrier, F., Kjeldsen, H., Bedding, T. R., et al. 2007. Solar-like oscillations in the metal-poor subgiant  $\nu$  Indi. II. Acoustic spectrum and mode lifetime. *A&A*, **470**, 1059.
- Carrier, F., De Ridder, J., Baudin, F., et al. 2010. Non-radial oscillations in the red giant HR 7349 measured by CoRoT. *A&A*, **55**, A73.
- Chaplin, W. J., Elsworth, Y., Isaak, G. R., et al. 1997. Solar p-mode linewidths from recent BiSON helioseismological data. *MNRAS*, **288**, 623.
- Chaplin, W. J., Appourchaux, T., Arentoft, T., et al. 2008a. AsteroFLAG: First results from hare-and-hounds Exercise #1. *Astron. Nachr.*, **329**, 549.
- Chaplin, W. J., Houdek, G., Appourchaux, T., et al. 2008b. Challenges for asteroseismic analysis of Sun-like stars. *A&A*, **485**, 813.
- Chaplin, W. J., Appourchaux, T., Elsworth, Y., et al. 2010. The Asteroseismic Potential of Kepler: First Results for Solar-Type Stars. *ApJ (Letters)*, **713**, L169.
- Chaplin, W. J., Kjeldsen, H., Christensen-Dalsgaard, J., et al. 2011. Ensemble Asteroseismology of Solar-Type Stars with the NASA Kepler Mission. *Science*, **332**, 213.
- Christensen-Dalsgaard, J. 1984. What will asteroseismology teach us? Page 11 of: Mangeney, A. & Praderie, F. (eds), *Workshop on Space Research in Stellar Activity and Variability*. Meudon: Observatoire de Paris.
- Christensen-Dalsgaard, J. 2004. Physics of solar-like oscillations. *Sol. Phys.*, **220**, 137.
- Christensen-Dalsgaard, J. 2008a. ASTEC – the Aarhus STellar Evolution Code. *Ap&SS*, **316**, 13.

- Christensen-Dalsgaard, J. 2008b. ADIPLS – the Aarhus adiabatic oscillation package. *Ap&SS*, **316**, 113.
- Christensen-Dalsgaard, J. 2011. Red giant asteroseismology. In: Pallé, P. L. (ed), *Asteroseismology*. Canary Islands Winter School of Astrophysics, vol. XXII. Cambridge University Press. in press (this volume; see arXiv:1106.5946).
- Christensen-Dalsgaard, J. & Houdek, G. 2010. Prospects for asteroseismology. *Ap&SS*, **328**, 51.
- Christensen-Dalsgaard, J., Däppen, W., & Lebreton, Y. 1988. Solar oscillation frequencies and the equation of state. *Nat*, **336**, 634.
- Christensen-Dalsgaard, J., Bedding, T. R., & Kjeldsen, H. 1995. Modeling solar-like oscillations in  $\eta$  Bootis. *ApJ*, **443**, L29.
- Christensen-Dalsgaard, J., Kjeldsen, H., & Mattei, J. A. 2001. Solar-like oscillations of semiregular variables. *ApJ*, **562**, L141.
- Cunha, M. S., Aerts, C., Christensen-Dalsgaard, J., et al. 2007. Asteroseismology and interferometry. *A&AR*, **14**, 217.
- De Ridder, J., Barban, C., Baudin, F., et al. 2009. Non-radial oscillation modes with long lifetimes in giant stars. *Nature*, **459**, 398.
- Degroote, P., Briquet, M., Catala, C., et al. 2009. Evidence for nonlinear resonant mode coupling in the  $\beta$  Cephei star HD 180642 (V1449 Aquilae) from CoRoT photometry. *A&A*, **506**, 111.
- Degroote, P., Briquet, M., Auvergne, M., et al. 2010. Detection of frequency spacings in the young O-type binary HD 46149 from CoRoT photometry. *A&A*.
- Deheuvels, S. & Michel, E. 2010a. New insights on the interior of solar-like pulsators thanks to CoRoT: the case of HD 49385. *Ap&SS*, **328**, 259.
- Deheuvels, S. & Michel, E. 2010b. Constraints on the core  $\mu$ -gradient of the solar-like star HD 49385 via low-degree mixed modes. *Astron. Nachr.*, **331**, 929.
- Deheuvels, S., Bruntt, H., Michel, E., et al. 2010. Seismic and spectroscopic characterization of the solar-like pulsating CoRoT target HD 49385. *A&A*. submitted.
- Di Mauro, M. P., Christensen-Dalsgaard, J., Kjeldsen, H., Bedding, T. R., & Paternò, L. 2003a. Convective overshooting in the evolution and seismology of  $\eta$  Bootis. *A&A*, **404**, 341.
- Di Mauro, M. P., Christensen-Dalsgaard, J., & Paternò, L. 2003b. A study of the solar-like properties of  $\beta$  Hydri. *Ap&SS*, **284**, 229.
- Di Mauro, M. P., Cardini, D., Catanzaro, G., et al. 2011. Solar-like oscillations from the depths of the red-giant star KIC 4351319 observed with *Kepler*. *MNRAS*. submitted.
- Dupret, M., Belkacem, K., Samadi, R., et al. 2009. Theoretical amplitudes and lifetimes of non-radial solar-like oscillations in red giants. *A&A*, **506**, 57.
- Dziembowski, W. A. & Pamyatnykh, A. A. 1991. A potential asteroseismological test for convective overshooting theories. *A&A*, **248**, L11.
- Dziembowski, W. A., Paternò, L., & Ventura, R. 1988. How comparison between observed and calculated p-mode eigenfrequencies can give information on the internal structure of the sun. *A&A*, **200**, 213.

- Dziembowski, W. A., Gough, D. O., Houdek, G., & Sienkiewicz, R. 2001. Oscillations of  $\alpha$  UMa and other red giants. *MNRAS*, **328**, 601.
- Edmonds, P. D. & Gilliland, R. L. 1996. K giants in 47 Tucanae: Detection of a new class of variable stars. *ApJ*, **464**, L157.
- Elsworth, Y., Howe, R., Isaak, G. R., McLeod, C. P., & New, R. 1990. Evidence from solar seismology against non-standard solar-core models. *Nature*, **347**, 536.
- Fernandes, J. & Monteiro, M. J. P. F. G. 2003. HR diagram and asteroseismic analysis of models for beta Hydri. *A&A*, **399**, 243.
- Fletcher, S. T., Chaplin, W. J., Elsworth, Y., Schou, J., & Buzasi, D. 2006. Frequency, splitting, linewidth and amplitude estimates of low-l p modes of  $\alpha$  Cen A: analysis of Wide-Field Infrared Explorer photometry. *MNRAS*, **371**, 935.
- Frandsen, S., Jones, A., Kjeldsen, H., et al. 1995. CCD photometry of the  $\delta$ -Scuti star  $\kappa^2$  Bootis. *A&A*, **301**, 123.
- Frandsen, S., Carrier, F., Aerts, C., et al. 2002. Detection of Solar-like oscillations in the G7 giant star xi Hya. *A&A*, **394**, L5.
- Fridlund, M., Gough, D. O., Jones, A., et al. 1994. STARS: A Proposal for a Dedicated Space Mission to Study Stellar Structure and Evolution. Page 416 of: Ulrich, R. K., Rhodes, Jr, E. J., & Däppen, W. (eds), *GONG '94: Helio- and Astero-seismology from Earth and Space*. ASP Conf. Ser.
- García, R. A., Jiménez, A., Mathur, S., et al. 2008. Update on g-mode research. *Astronomische Nachrichten*.
- García, R. A., Regulo, C., Samadi, R., et al. 2009. Solar-like oscillations with low amplitude in the CoRoT target HD 181906. *A&A*, **506**, 41.
- Gastine, T. & Dintrans, B. 2011. Convective quenching of stellar pulsations. *A&A*, **528**, A6.
- Gilliland, R. L. 2008. Photometric Oscillations of Low-Luminosity Red Giant Stars. *AJ*, **136**, 566.
- Gilliland, R. L., Brown, T. M., Kjeldsen, H., et al. 1993. A search for solar-like oscillations in the stars of M67 with CCD ensemble photometry on a network of 4 m telescopes. *AJ*, **106**, 2441.
- Gilliland, R. L., Jenkins, J. M., Borucki, W. J., et al. 2010a. Initial Characteristics of Kepler Short Cadence Data. *ApJ (Letters)*, **713**, L160.
- Gilliland, R. L., Brown, T. M., Christensen-Dalsgaard, J., et al. 2010b. Kepler Asteroseismology Program: Introduction and First Results. *PASP*, **122**, 131–143.
- Gilliland, R. L., McCullough, P. R., Nelan, E. P., et al. 2011. Asteroseismology of the Transiting Exoplanet Host HD 17156 with Hubble Space Telescope Fine Guidance Sensor. *ApJ*, **726**, 2.
- Girardi, L. 1999. A secondary clump of red giant stars: why and where. *MNRAS*, **308**, 818–832.
- Gough, D. O. 1986. EBK Quantization of Stellar Waves. Page 117 of: Osaki, Y. (ed), *Hydrodynamic and Magnetodynamic Problems in the Sun and Stars*. Tokyo: Uni. of Tokyo Press.
- Gough, D. O. 2001. The Birth of Asteroseismology. *Science*, **291**, 2325.

- Gough, D. O. 2003. On the Principal Asteroseismic Diagnostic Signatures. *Ap&SS*, **284**, 165.
- Grec, G., Fossat, E., & Pomerantz, M. A. 1983. Full-disk observations of solar oscillations from the geographic South Pole: latest results. *Sol. Phys.*, **82**, 55.
- Grigahcène, A., Antoci, V., Balona, L., et al. 2010. Hybrid  $\gamma$  Doradus- $\delta$  Scuti Pulsators: New Insights into the Physics of the Oscillations from Kepler Observations. *ApJ*, **713**, L192.
- Grundahl, F., Kjeldsen, H., Frandsen, S., et al. 2006. SONG: Stellar Oscillations Network Group . A global network of small telescopes for asteroseismology and planet searches. *Mem. Soc. Astron. Ital.*, **77**, 458.
- Guenther, D. B. 2004. Quantitative Analysis of the Oscillation Spectrum of  $\eta$  Bootis. *ApJ*, **612**, 454.
- Guenther, D. B. & Demarque, P. 1996. Seismology of  $\eta$  Bootis. *ApJ*, **456**, 798.
- Guenther, D. B., Demarque, P., Buzasi, D., et al. 2000. Evolutionary Model and Oscillation Frequencies for Ursae Majoris: A Comparison with Observations. *ApJ*, **530**, L45.
- Heasley, J. N., Janes, K., Labonte, B., et al. 1996. The Prospects for Asteroseismology from Ground-based Sites. *PASP*, **108**, 385.
- Hekker, S. 2010. Observations and interpretation of solar-like oscillations in red-giant stars. *Astron. Nachr.*, **331**, 1004.
- Hekker, S., Kallinger, T., Baudin, F., et al. 2009. Characteristics of solar-like oscillations in red giants observed in the CoRoT exoplanet field. *A&A*, **506**, 465.
- Hekker, S., Barban, C., Baudin, F., et al. 2010. Oscillation mode lifetimes of red giants observed during the initial and first anticentre long run of CoRoT. *A&A*, **520**, A60.
- Hekker, S., Basu, S., Stello, D., et al. 2011a. Asteroseismic inferences on red giants in open clusters NGC 6791, NGC 6819, and NGC 6811 using Kepler. *A&A*, **530**, A100.
- Hekker, S., Gilliland, R. L., Elsworth, Y., et al. 2011b. Characterization of red giant stars in the public Kepler data. *MNRAS*. in press.
- Hekker, S., Elsworth, Y., De Ridder, J., et al. 2011c. Solar-like oscillations in red giants observed with Kepler: comparison of global oscillation parameters from different methods. *A&A*, **525**, A131.
- Huber, D., Bedding, T. R., Stello, D., et al. 2010. Asteroseismology of Red Giants from the First Four Months of Kepler Data: Global Oscillation Parameters for 800 Stars. *ApJ*, **723**, 1607.
- Huber, D., Bedding, T. R., Arentoft, T., et al. 2011a. Solar-like Oscillations and Activity in Procyon: A Comparison of the 2007 MOST and Ground-based Radial Velocity Campaigns. *ApJ*, **731**, 94.
- Huber, D., Bedding, T. R., Stello, D., et al. 2011b. Testing Scaling Relations for Solar-Like Oscillations from the Main-Sequence to Red Giants using *Kepler* Data. *ApJ*. submitted.

- Jenkins, J. M., Caldwell, D. A., Chandrasekaran, H., et al. 2010. Initial Characteristics of *Kepler* Long Cadence Data for Detecting Transiting Planets. *ApJ* (Letters), **713**, L120.
- Kallinger, T. & Matthews, J. M. 2010. Evidence for Granulation in Early A-Type Stars. *ApJ*, **711**, L35.
- Kallinger, T., Zwintz, K., Pamyatnykh, A. A., Guenther, D. B., & Weiss, W. W. 2005. Pulsation of the K 2.5 giant star GSC 09137-03505? *A&A*, **433**, 267.
- Kallinger, T., Mosser, B., Hekker, S., et al. 2010a. Asteroseismology of red giants from the first four months of Kepler data: Fundamental stellar parameters. *A&A*, **522**, A1.
- Kallinger, T., Weiss, W. W., Barban, C., et al. 2010b. Oscillating Red Giants in the CoRoT Exo-field: Asteroseismic Radius and Mass Determination. *A&A*, **509**, A77.
- Kambe, E., Ando, H., Sato, B., et al. 2008. Development of Iodine Cells for the Subaru HDS and the Okayama HIDES: III. An Improvement on Radial Velocity Measurement Technique. *PASJ*, **60**, 45.
- Kiss, L. L., Szabo, G. M., & Bedding, T. R. 2006. Variability in red supergiant stars: pulsations, long secondary periods and convection noise. *MNRAS*, **372**, 1721.
- Kjeldsen, H. & Bedding, T. R. 1995. Amplitudes of stellar oscillations: the implications for asteroseismology. *A&A*, **293**, 87.
- Kjeldsen, H., Bedding, T. R., Viskum, M., & Frandsen, S. 1995. Solar-like oscillations in  $\eta$  Boo. *AJ*, **109**, 1313.
- Kjeldsen, H., Bedding, T. R., Frandsen, S., & Dall, T. H. 1999. A search for solar-like oscillations and granulation in  $\alpha$  Cen A. *MNRAS*, **303**, 579.
- Kjeldsen, H., Bedding, T. R., & Christensen-Dalsgaard, J. 2000. MONS: Measuring Oscillations in Nearby Stars. Page 73 of: Szabados, L. & Kurtz, D. (eds), *IAU Colloquium 176: The Impact of Large-Scale Surveys on Pulsating Star Research*, vol. 203. ASP Conf. Ser.
- Kjeldsen, H., Bedding, T. R., Baldry, I. K., et al. 2003. Confirmation of Solar-Like Oscillations in  $\eta$  Bootis. *AJ*, **126**, 1483.
- Kjeldsen, H., Bedding, T. R., Butler, R. P., et al. 2005. Solar-like oscillations in  $\alpha$  Centauri B. *ApJ*, **635**, 1281.
- Kjeldsen, H., Bedding, T. R., & Christensen-Dalsgaard, J. 2008. Correcting stellar oscillation frequencies for near-surface effects. *ApJ*, **683**, L175.
- Li, L. H., Robinson, F. J., Demarque, P., Sofia, S., & Guenther, D. B. 2002. Inclusion of Turbulence in Solar Modeling. *ApJ*, **567**, 1192.
- Martić, M., Schmitt, J., Lebrun, J.-C., et al. 1999. Evidence for global pressure oscillations on Procyon. *A&A*, **351**, 993.
- Martić, M., Lebrun, J.-C., Appourchaux, T., & Korzenik, S. G. 2004. p-mode frequencies in solar-like stars. I. Procyon A. *A&A*, **418**, 295.
- Mathur, S., García, R. A., Catala, C., et al. 2010a. The solar-like CoRoT target HD 170987: spectroscopic and seismic observations. *A&A*, **518**, A53.

- Mathur, S., García, R. A., Catala, C., et al. 2010b. The solar-like CoRoT target HD 170987: spectroscopic and seismic observations. *A&A*, **518**, A53.
- Mathur, S., Handberg, R., Campante, T. L., et al. 2011. Solar-like Oscillations in KIC 11395018 and KIC 11234888 from 8 Months of Kepler Data. *ApJ*, **733**, 95.
- Matthews, J. M., Kuschnig, R., Guenther, D. B., et al. 2004. No stellar p-mode oscillations in space-based photometry of Procyon. *Nat*, **430**, 51. Erratum: 430, 921.
- Metcalf, T. S., Monteiro, M. J. P. F. G., Thompson, M. J., et al. 2010. A Precise Asteroseismic Age and Radius for the Evolved Sun-like Star KIC 11026764. *ApJ*, **723**, 1583.
- Michel, E., Baglin, A., Auvergne, M., et al. 2008. CoRoT measures solar-like oscillations and granulation in stars hotter than the Sun. *Science*, **322**, 558.
- Miglio, A., Montalbán, J., Eggenberger, P., & Noels, A. 2008. Gravity modes and mixed modes as probes of stellar cores in main-sequence stars: From solar-like to  $\beta$  Cep stars. *Astronomische Nachrichten*, **329**, 529–534.
- Miglio, A., Montalbán, J., Baudin, F., et al. 2009. Probing populations of red giants in the galactic disk with CoRoT. *A&A*, **503**, L21.
- Montalbán, J., Miglio, A., Noels, A., Scuflaire, R., & Ventura, P. 2010. Seismic Diagnostics of Red Giants: First Comparison with Stellar Models. *ApJ (Letters)*, **721**, L182.
- Mosser, B., Maillard, J. P., Mékarnia, D., & Gay, J. 1998. New limit on the p-mode oscillations of Procyon obtained by Fourier transform seismometry. *A&A*, **340**, 457.
- Mosser, B., Michel, E., Appourchaux, T., et al. 2009. The CoRoT target HD 175726: an active star with weak solar-like oscillations. *A&A*, **506**, 33.
- Mosser, B., Belkacem, K., Goupil, M., et al. 2010. Red-giant seismic properties analyzed with CoRoT. *A&A*, **517**, A22.
- Mosser, B., Barban, C., Montalbán, J., et al. 2011a. Mixed modes in red-giant stars observed with CoRoT. *A&A*. in press (arXiv:1105.6113).
- Mosser, B., Belkacem, K., Goupil, M. J., et al. 2011b. The universal red-giant oscillation pattern. An automated determination with CoRoT data. *A&A*, **525**, L9.
- Orwell, G. 1945. *Animal Farm*. Secker and Warburg (London).
- Osaki, J. 1975. Nonradial oscillations of a 10 solar mass star in the main-sequence stage. *PASJ*, **27**, 237–258.
- Pérez Hernández, F. & Christensen-Dalsgaard, J. 1998. The phase function for stellar acoustic oscillations - IV. Solar-like stars. *MNRAS*, **295**, 344.
- Pijpers, F. P. 2006. *Methods in helio- and asteroseismology*. Imperial College Press.
- Reed, M. D., Baran, A., Quint, A. C., et al. 2011. First Kepler results on compact pulsators VIII: Mode identifications via period spacings in  $g$ -mode pulsating Subdwarf B stars. *MNRAS*. in press (arXiv:1102.4286).
- Retter, A., Bedding, T. R., Buzasi, D., Kjeldsen, H., & Kiss, L. L. 2003. Arcturus. *ApJ*, **591**, L151.

- Rosenthal, C. S., Christensen-Dalsgaard, J., Nordlund, Å., Stein, R. F., & Trampedach, R. 1999. Convective contributions to the frequencies of solar oscillations. *A&A*, **351**, 689.
- Roxburgh, I. W. 2010. Asteroseismology of solar and stellar models. *Ap&SS*, **328**, 3.
- Roxburgh, I. & Favata, F. 2003. The Eddington Mission. *Ap&SS*, **284**, 17.
- Samadi, R., Goupil, M.-J., & Houdek, G. 2002. Solar-like oscillations in  $\delta$  Scuti stars. *A&A*, **395**, 563.
- Schou, J. & Buzasi, D. L. 2001. Observations of p-modes in  $\alpha$  Cen. Page 391 of: *Helio- and Asteroseismology at the Dawn of the Millenium, Proc. SOHO 10/GONG 2000 Workshop*. ESA SP-464.
- Scuflaire, R. 1974. The Non Radial Oscillations of Condensed Polytropes. *A&A*, **36**, 107.
- Smith, M. A. 1982. Precise radial velocities. I - A preliminary search for oscillations in Arcturus. *ApJ*, **253**, 727.
- Stello, D. & Gilliland, R. L. 2009. Solar-like Oscillations in a Metal-poor Globular Cluster with the Hubble Space Telescope. *ApJ*, **700**, 949.
- Stello, D., Bruntt, H., Preston, H., & Buzasi, D. 2008. Oscillating K Giants with the WIRE Satellite: Determination of Their Asteroseismic Masses. *ApJ*, **674**, L53.
- Stello, D., Chaplin, W. J., Basu, S., Elsworth, Y., & Bedding, T. R. 2009. The relation between  $\Delta\nu$  and  $\nu_{\max}$  for solar-like oscillations. *MNRAS*, **400**, L80.
- Stello, D., Basu, S., Bruntt, H., et al. 2010. Detection of Solar-like Oscillations from Kepler Photometry of the Open Cluster NGC 6819. *ApJ (Letters)*, **713**, L182.
- Tabur, V., Bedding, T. R., Kiss, L. L., et al. 2010. Period-luminosity relations of pulsating M giants in the solar neighbourhood and the Magellanic Clouds. *MNRAS*, **409**, 777.
- Tarrant, N. J., Chaplin, W. J., Elsworth, Y., Sreckley, S. A., & Stevens, I. R. 2007. Asteroseismology of red giants: photometric observations of Arcturus by SMEI. *MNRAS*, **382**, L48.
- Tarrant, N. J., Chaplin, W. J., Elsworth, Y., Sreckley, S. A., & Stevens, I. R. 2008. Oscillations in  $\beta$  Ursae Minoris. Observations with SMEI. *A&A*, **483**, L43.
- Tassoul, M. 1980. Asymptotic approximations for stellar nonradial pulsations. *ApJS*, **43**, 469.
- Traub, W. A., Mariska, J. T., & Carleton, N. P. 1978. A search for stellar oscillations. *ApJ*, **223**, 583.
- Vauclair, S., Laymand, M., Bouchy, F., et al. 2008. The exoplanet-host star  $\iota$  Horologii: an evaporated member of the primordial Hyades cluster. *A&A*, **482**, L5.
- Verner, G. A., Elsworth, Y., Chaplin, W. J., et al. 2011. Global asteroseismic properties of solar-like oscillations observed by Kepler : A comparison of complementary analysis methods. *MNRAS*. in press (arXiv:1105.0571).
- Walker, G., Matthews, J., Kuschnig, R., et al. 2003. The MOST asteroseismology mission: ultraprecise photometry from space. *PASP*, **115**, 1023.



- White, T. R., Bedding, T. R., Stello, D., et al. 2011. Calculating asteroseismic diagrams for solar-like oscillations. *ApJ*. submitted.
- Zwintz, K., Kuschnig, R., Weiss, W. W., Gray, R. O., & Jenkner, H. 1999. Hubble Deep Field guide star photometry. *A&A*, **343**, 899.